Development of Stack Model for Tri-Electrode Rechargeable
Zinc-Air Cylindrical Flow Battery

Miss Kanya Bumroongsil

จุฬาลงกรณ์มหาวิทยาลัย
CHULALONGKORN UNIVERSITY

A Thesis Submitted in Partial Fulfillment of the Requirements
for the Degree of Master of Engineering in Chemical Engineering
Department of Chemical Engineering
Faculty of Engineering
Chulalongkorn University
Academic Year 2019
Copyright of Chulalongkorn University

การพัฒนาแบบจำลองสแต็คสำหรับแบตเตอรี่สังกะสี-อากาศแบบไหลในท่อชนิดสามขั้วซึ่งอัด
ประจุซ้ำได้

น.ส.กันยา บำรุงศิลป์

จุฬาลงกรณ์มหาวิทยาลัย
CHULALONGKORN UNIVERSITY

วิทยานิพนธ์นี้เป็นส่วนหนึ่งของการศึกษาตามหลักสูตรปริญญาวิศวกรรมศาสตรมหาบัณฑิต
สาขาวิชาวิศวกรรมเคมี ภาควิชาวิศวกรรมเคมี
คณะวิศวกรรมศาสตร์ จุฬาลงกรณ์มหาวิทยาลัย
ปีการศึกษา 2562
ลิขสิทธิ์ของจุฬาลงกรณ์มหาวิทยาลัย

Thesis Title   Development of Stack Model for Tri-Electrode
         Rechargeable Zinc-Air Cylindrical Flow Battery
By   Miss Kanya Bumroongsil
Field of Study   Chemical Engineering
Thesis Advisor   Associate Professor SOORATHEP KHEAWHOM,
         Ph.D.

   Accepted by the Faculty of Engineering, Chulalongkorn University in Partial Fulfillment of the Requirement for the Master of Engineering

                Dean of the Faculty of Engineering
    (Professor SUPOT TEACHAVORASINSKUN, D.Eng.)

THESIS COMMITTEE
                Chairman
    (Professor SARAWUT RIMDUSIT, Ph.D.)
                Thesis Advisor
    (Associate Professor SOORATHEP KHEAWHOM,
    Ph.D.)
                Examiner
    (PIMPORN PONPESH, Ph.D.)
                External Examiner
    (Assistant Professor Pornchai Bumroongsri, D.Eng.)

จุฬาลงกรณ์มหาวิทยาลัย

CHULALONGKORN UNIVERSITY

กันยา บำรุงศิลป์ : การพัฒนาแบบจำลองสแต็คสำหรับแบตเตอรี่สังกะสี-อากาศแบบไหลในท่อชนิดสามขั้วซึ่งอัด
ประจุซ้ำได้. (Development of Stack Model for Tri-Electrode Rechargeable
Zinc-Air Cylindrical Flow Battery) อ.ที่ปรึกษาหลัก : รศ. ดร.สุรเทพ เขียวหอม

　　　　　ปัจจุบันความต้องการพลังงานทดแทนมีเพิ่มขึ้นอย่างต่อเนื่อง　ดังนั้นระบบกักเก็บพลังงานที่มีประสิทธิภาพจึงมี
ความสำคัญอย่างมาก แบตเตอรี่สังกะสี-อากาศได้รับความสนใจกันอย่างกว้างขวาง เนื่องจากใช้วัตถุดิบที่มีราคาถูกอีกทั้งยังเป็น
ระบบที่มีความปลอดภัยสูง งานวิจัยนี้จึงทำการพัฒนาแบบจำลองสแต็คสำหรับแบตเตอรี่สังกะสี-อากาศแบบไหลในท่อชนิด
สามขั้วซึ่งอัดประจุซ้ำได้ขึ้น เพื่อนำไปใช้งานในระบบที่มีขนาดใหญ่ โดยศึกษาการนำเซลล์แบตเตอรี่มาต่อกันทั้งแบบอนุกรม
และแบบขนาน การต่อเซลล์แบตเตอรี่แบบอนุกรมและมีการไหลของอิเล็คโตรไลต์ร่วมกันทำให้เกิดกระแสชันท์ขึ้น แบบจำลอง
ที่สร้างขึ้นถูกนำไปสอบเทียบด้วยผลการทดลองซึ่งวัดทั้งแรงดันเต็มเซลล์และแรงดันครึ่งเซลล์ แบบจำลองที่ได้มีความสอดคล้อง
กับผลการทดลอง จากนั้นได้วิเคราะห์ผลกระทบของตัวแปรต่างๆ ต่อการเกิดกระแสชันท์ พบว่าเมื่อเพิ่มอัตราการไหลของอิเล็ค
โตรไลต์ จะไม่มีผลกับขนาดของกระแสชันท์ที่เกิดขึ้น แต่ช่วยเพิ่มประสิทธิภาพเชิงประจุในการอัดประจุอย่างมาก แต่ลด
ประสิทธิภาพเชิงประจุในการคายประจุ เมื่อเพิ่มความหนาแน่นกระแส ขนาดของกระแสชันท์ลดลงทั้งการอัดประจุและคาย
ประจุ ประสิทธิภาพเชิงประจุในการคายประจุเพิ่มขึ้น แต่ประสิทธิภาพเชิงประจุในการอัดประจุลดลง ทั้งนี้ประสิทธิภาพเชิง
ประจุของเซลล์แบตเตอรี่ที่ต่อกันแบบอนุกรม สามารถเพิ่มขึ้นได้ด้วยการเพิ่มความต้านทานเสมือนในเส้นทางการไหลของอิเล็ค
โตรไลต์ ดังนั้นการต่อเซลล์จำนวนมากขึ้นแบบอนุกรมแม้จะให้ศักย์ไฟฟ้าที่สูงขึ้นแต่ก็ทำให้เกิดกระแสชันท์มากขึ้นเช่นกัน การ
ต่อเซลล์แบบขนาน ไม่มีผลต่อการเกิดกระแสชันท์แต่กระแสที่แบ่งไปให้แต่ละเซลล์จะมีค่าไม่เท่ากันขึ้นอยู่กับความต้านทาน
ภายในของแต่ละเซลล์

สาขาวิชา	วิศวกรรมเคมี	ลายมือชื่อนิสิต ....
ปีการศึกษา	2562	ลายมือชื่อ อ.ที่ปรึกษาหลัก ....

Kanya Bumroongsil : Development of Stack Model for Tri-Electrode Rechargeable Zinc-Air Cylindrical Flow Battery. Advisor: Assoc. Prof. SOORATHEP KHEAWHOM, Ph.D.

Nowadays, the demand for renewable energy is continuously increasing. Therefore, an efficient energy storage system is essential. Zinc-air batteries have received extensive attention because they use low-cost material but offer great safety benefits. This research, therefore, develops a stack model for a tri-electrode tubular designed rechargeable zinc-air flow battery for using in a large scale system. The connection of battery cells in series and parallel is studied. The connection of battery cell with common flowing electrolyte creates a shunt current. A mathematical model is developed and validated against experimental data, which measured both full cell and half cell potentials. The model agrees well with the experimental results. After that, the model is used to examine the effects of various parameters on the shunt current. Results show that increasing the electrolyte flow rate does not affect the shunt current. It enhances the coulombic efficiency of the charging process and decreases the coulombic efficiency of the discharging process. By increasing the current density, the shunt currents for both charging and discharging processes decrease; the coulombic efficiency of the discharging process increases; the coulombic efficiency of the charging process decreases. The coulombic efficiency of series-connected cells can be improved by increasing the pseudo resistance of the flowing electrolyte. It can be concluded that, by connecting the cells in series, the output potential of the module can be enhanced but the shunt current is also increased. By connecting the cells in parallel, though the shunt current is not observed, the current flow to each cell is not identical but determined by its internal resistivity.

จุฬาลงกรณ์มหาวิทยาลัย
CHULALONGKORN UNIVERSITY

Field of Study:	Chemical Engineering	Student's Signature	....
Academic Year:	2019	Advisor's Signature	....

ACKNOWLEDGEMENTS

จุฬาลงกรณ์มหาวิทยาลัย
CHULALONGKORN UNIVERSITY

TABLE OF CONTENTS

Page

Chapter 1

Introduction

1.1 Background

Nowadays, the demand of energy storage is increasing in order to supply the electronic device industry especially electric vehicles (EVs). This is the reason why the battery has to be developed the performance, energy density, cost and the most important is environment-friendly. Because of lots of usability, there are lots of waste. Thus, the development of energy storage in the present focus on renewable energy by using them as a raw material. The main problem of renewable energy such as solar power is its instability. A long-life rechargeable battery is required for supply energy. Metal-air batteries are a good choice for eco-battery. Air is used to generate energy then store it in the battery. In terms of metal, zinc is preferable. There are many zinc-metals in nature. It is inexpensive, environmentally safe and recyclable. Moreover, the zinc-air battery has high energy density and low cost of raw material, so it can be used instead of lithium-ion batteries in EVs.

Zinc-air battery consists of air electrode, zinc electrode, separator, and alkaline electrolyte. The basic principle of this battery is electrochemically oxidizing the zinc electrode in anode and reducing oxygen from air in cathode. The reactions in the discharging process occur as follows in table 1.1. And charging reactions will occur in the opposite direction. Currently, the primary zinc-air battery has been used in commercials such as hearing aids, navigation lights, and railway signals. Rechargeable zinc-air batteries still have lots of problems. It has practical energy density much lower than theoretical energy density. So, it has been being developed before approaching the commercial scale.

Table.1.1 Reaction in the zinc-air battery during discharge

No.	Reaction	Equation
(1.1)	Oxygen reduction reaction (cathode)	$\frac{1}{2}O_2 + H_2O + 2e^- \leftrightarrow 2OH^-$
(1.2)	Dissolution (anode)	$Zn + 4OH^- \leftrightarrow Zn(OH)_4{}^{2-} + 2e^-$
(1.3)	Precipitation	$Zn(OH)_4{}^{-2} \leftrightarrow ZnO + 2OH^- + H_2O$
(1.4)	Overall reaction	$2Zn + O_2 \leftrightarrow 2ZnO$
(1.5)	Hydrogen evolution reaction	$2H_2O + 2e^- \rightarrow H_2 + 2OH^-$
(1.6)	Parasitic reaction	$Zn + 2OH^- + 2H_2O \rightarrow Zn(OH)_4{}^{-2} + H_2$

There are many points that have to be resolved including dendritic growth for zinc regeneration, passivation, degradation of air electrode and hydrogen evolution reaction (HER). While charging the battery, dendritic growth of zinc-metal results from diffusion-controlled on the zinc-electrode surface boundary. They can puncture separator then short-circuit (Riede, Turek et al. 2018). On the other hand, passivation will occur in the zinc electrode during discharging the battery. Precipitation reaction forms a layer of oxy-products from reaction (1.3) covering the electrode surface which causes active zinc from dissolution reaction to become passive (Bockelmann, Reining et al. 2017). As for air-electrode, it consists of gas diffusion layer and catalytic layer because oxygen reduction reaction (ORR) will occur at triple-phase boundary according to reaction (1.1) in table 1.1. So, the construction of air electrode has to be balanced hydrophobic and hydrophilic properties. Moreover, both layers are easy to be damaged by bubble producing from oxygen evolution reaction (OER), reversing of reaction (1.1), during recharge the battery. Another problem is HER which leads to a parasitic reaction on the zinc electrode showed in reaction (1.6). It consumes electrolyte and zinc leading to self-corrosion and reduces zinc utilization on the anode (Li and Dai 2014).

Previous researches found the method to solve these problems. First, in case of charging process, the low current and flowing electrolyte can inhibit dendrite formation on the zinc electrode by enhancing zinc-ion diffusion (Wang, Pei et al. 2014). Because of diffusion-limited control at late stage of zinc deposition, the morphology becomes stems instead of boulder (Wang, Pei et al. 2015). Also, forced convection by flowing electrolyte in the battery can solve the zinc passivation problem while discharge by reducing the concentration gradient of hydroxide ion on the surface of the zinc electrode (Bockelmann, Reining et al. 2017). In case of charging process, flowing electrolyte also inhibits bubble coalescence from OER which can prevent bubble blocking on active area. For another, three-electrode configuration can retard the degradation of the air electrode. Zinc-electrode will be connected to air-electrode for ORR while charging and connected to third-electrode while discharge. This configuration can improve cycling stability of the battery (Li and Dai 2014). As for HER, adding zinc oxide into electrolyte can suppress the HER and increase the current efficiency of the battery (Lao-atiman, Bumroongsil et al. 2019). Many attempts of experiment for finding the optimum operating condition. High coulombic efficiencies (80%-93%) were found for 0.5 M ZnO in 8 M KOH at current densities up to 100 mA/cm^2 with electrolyte flow (Gavrilovic-Wohlmuther, Laskos et al. 2015).

In addition, previous studies had developed theory-based models of metal-air battery in order to investigate the behavior of battery for researchers' understanding of complex electrochemical systems. Zero-dimension model of the secondary zinc-air battery had developed to investigate the influence of air composition (Schröder and Krewer 2014). They found the impact of humidity, carbon dioxide, and oxygen. Moreover, the basic model can be used for investigating zinc-air battery. But Schröder and Krewer's model did not consider the parasitic reaction or HER in the battery.

HER had introduced in the model from Deiss, Holzer, et al. 2002 in one-dimension of zinc paste electrode form. And then from Jan Dundáleka et al. 2017 work, they investigate the influence of this reaction even though they focus on electrolyzer only. Zinc-air flow battery and zinc electrolyzer including HER had introduced (Lao-atiman, Bumroongsil et al. 2019). This model was more realistic, but it was still separated from the battery into two parts. One was battery for discharge. Another was electrolyzer for zinc regeneration. Most studies have focused on single-cell scale. Scaling up the battery is necessary to supply enough energy. Battery with flowing electrolyte systems usually have an energy loss caused by leakage currents flowing along the manifold (Mu¨Ller, Haas et al. 1998). The shunt current problem was avoided by using separate electrolyte circuits, but it decreases the specific energy of the battery.

In this study, zero-dimension models of zinc-air flow battery and zinc electrolyzer will be modified to be a tri-electrode zinc-air battery with flowing electrolyte mathematics model. Each cell is fabricated in a tube and connected in series. The new model configuration is more commercialized. This research aims to study the effect of shunt current on each cell when connected in series. The current and potential in each cell of battery which depends on time are studied. So, the maximum power evaluated by the polarization curve will provide a suitable operating condition.

1.2 Objective

1.2.1 To develop a tri-electrode zinc-air battery with flowing electrolyte model.

1.2.2 To study the effect of shunt current on each cell when connected in series and parallel.

1.2.3 To study the coulombic efficiency of the scaling up battery, charge and discharge processes, to evaluate the battery performance.

1.3 Scope of research

1.3.1 The model is simulated by MATLAB.

1.3.4 The model is validated by the experiment of a single-cell zinc-air battery.

1.3.5 The designed components and parameters are depicted in table 1.2, 1.3.

1.3.6 The studied parameters are the number of cells connected in series and parallel, current density for charge and discharge the battery and electrolyte flow rate. The value is showed in table 1.4.

Table 1.2 Designed components of the battery

Component	Detail
Battery case	PVC
Air electrode current collector	Ni foam
Gas diffusion layer	PTFE 40%/Carbon 40%/D-glucose 20%
Catalytic layer	Carbon 70%/MnO$_2$ 30%
Zn electrode current collector	Ni foam
Third-electrode current collector	Ni foam
Electrolyte	KOH/ZnO
Separator	Polyvinyl acetate membrane

Table 1.3 Designed parameters of battery

Parameter	Value
Air electrode thickness	1.3 mm
Zn electrode thickness	1.1 mm
Third electrode thickness	1.1 mm
Separator thickness	0.2 mm
Electrolyte volume in single-cell battery	45 cm^3
Electrolyte tank volume	500 cm^3

Table 1.4 Studied parameters of the battery

Parameter	Value
Number of cells connected	2,3,4,5 cells
Current density for charge and discharge	10,25,50,75 mA/cm^2
Velocity of electrolyte	0.025, 0.25, 2.5, 25 cm/s
Electrolyte flow path resistance	5, 10, 20, 50 Ω

1.4 Research Framework

Table 1.5Research planning

No.	Activity	Jan	Feb	Mar	Apr	May	Jun	Jul	Aug	Sep	Oct	Nov
1.	Research the overview of Zn-Air battery	←——			——→							
2.	Conduct experiment of Zn-air flowing battery		←——		——→							
3.	Develop the model of Zn-air flowing battery			←——				——→				
4.	Study the shunt current phenomenon						←——		——→			
5.	Develop the battery model connected in series							←——	——→			
6.	Conduct experiments to find the constant parameter								←——		——→	
7.	Validate model							←——			——→	
8.	Study the effect of operating parameters of battery								←——			——→

Chapter 2

Theory and literature reviews

2.1 Battery configuration

The basic structure of the battery comprises of zinc electrode, air electrode, and separator assembled in an electrolyte. The zinc electrode is a negative electrode which consists of zinc-metal. The air electrode consists of the substrate that oxygen from surrounding can penetrate the porous surface to contact with water in the electrolyte and be reduced on the catalyst on the electrode. Thus, this positive electrode has two layers coated on the porous substrate. There are gas diffusion layer and catalytic layer (Li and Dai 2014). The configurations of the zinc-air battery have been introduced in many types. For a commercial product, primary cells for hearing aid button format has high energy density, but power output capability is low. Later, a mechanically rechargeable battery was developed by refilling fresh zinc-metals or feeding slurry zinc particles to the anode (Khor, Leung et al. 2018). Then, plate and tube format have been fabricated with non-flowing or flowing electrolyte and both formats are preferable because it does not complicate, easy to compose and clean. Each component of the zinc-air battery is discussed as follows.

2.1.1 Zinc electrode

In the commercial battery, the zinc electrode is zinc paste which is zinc powder suspended in the electrolyte by gel formation. The high surface area of zinc brings about high reaction rate. In the same way, the side reaction rate also increases creating the corrosion of zinc. The ways to suppress this are alloying zinc with other metals such as Ni to stabilize the zinc electrode. Pichler, Berner et al. investigated different current collector material (nickel, brass, and steel) by using Rota-Hull cylinders. It showed that nickel is the most suitable material for compact zinc deposition in a broad current density range without any electrolyte additive (Pichler, Berner et al. 2018). Also, coating electrode surface with a small of other materials such as Al_2O_3 or lithium boron oxide can reduce HER and increase discharging time similar to other additive and surfactant which can promote the formation of compact zinc deposit (Li and Dai 2014). For example, inorganic additives such as calcium hydroxide have been used to trap the zincate or discharge product to form the stable structure $CaZn_2(OH)_6 \cdot 2H_2O$ which has better electrochemical reversibility than ZnO. Therefore, this mechanism avoids zincate loss on the surface and can reduce shape change by using this material on the zinc electrode (Zhu, Yang et al. 2003). Furthermore, modification of zinc electrode with polymer can reduce dendrite formation and shape change such as coating polyaniline on the porous zinc electrode which allows hydroxide passing and restricts zincate but the problem of pore plugging of the polymer-coated electrode have to be improved (Vatsalarani, Trivedi et al. 2005).

2.1.2 Separator

The separator for zinc-air battery keeps apart negative electrode and positive electrode should have high adsorption of alkaline electrolyte. The important properties are low ionic resistance and high electrical resistance. As for the dendritic growth on the zinc electrode, separators should have strong structure to resist the perforation of zinc dendrite for safety and long cycle life of the battery. For this reason, organic polymer porous membranes can be commonly used as the separator in a zinc-air battery.

2.1.3 Electrolyte

Generally, zinc-air batteries operate in an alkaline electrolyte such as KOH and NaOH for higher activity of both zinc electrode and air electrode. KOH has better ionic conductivity, higher oxygen diffusion coefficients, and lower viscosity than NaOH. During operating, the reactions of KOH with CO_2 showed below (Equation 2.1 and 2.2) have to be concerned. In addition, the product K_2CO_3 or $KHCO_3$ have higher solubilities than their sodium counterparts. Therefore, using KOH instead of NaOH can delay the carbonate precipitation. According to Lao-atiman et al. research, the optimal KOH concentration is 6 and 7 M resulting in maximum discharge energy by simulated the zinc air battery model similar to other researches employed 7 M for its maximum conductivity (Li and Dai 2014).

$$2KOH + CO_2 \rightarrow K_2CO_3 + H_2O \qquad (2.1)$$

$$KOH + CO_2 \rightarrow KHCO_3 \qquad (2.2)$$
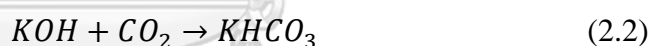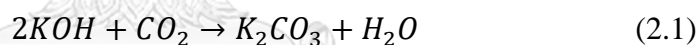
Also, carbonate formation still exists in the electrolyte and decreases conductivity and the precipitation of it leading to blocking pore of the electrode. As a result, the carbon dioxide sensitivity of alkaline electrolytes has to be suppressed by filtering it out from air by using simple inexpensive hydroxides scrubber such as soda-lime by passing the air through this filter before passing through the air electrode or adding additive into the electrolyte. For another purpose of additive, calcium hydroxide or silicate has been used to trap the zincate or discharge product for increasing the electrolyte capacity (Zhu, Duch et al. 2015).

Moreover, the open system affects water loss from the aqueous electrolyte which is the important cause of decreasing the performance of battery. Solid-state zinc-air batteries have been found to improve water loss by gel formation of electrolyte. Later, aprotic electrolytes such as ionic liquids have been proposed to slow down the drying-out of electrolyte, inhibit self-corrosion and eliminate its carbonation. In contrast, ionic liquids have high viscosity and hard to wet the air electrode decreasing voltage during discharge (Li and Dai 2014).

2.1.4 Air electrode

ORR occurs at triple-phase boundary where the solid electrode contacts with ion in the liquid electrolyte and gas phase. The air electrode development focus on performance and durability. According to figure 2.1, the gas diffusion layer (GDL) supplies reactant gas to the catalytic layer and prevents the electrolyte from passing through the electrode or flooding. Thus, the GDL side has to be hydrophobicity and porous. Its properties depend on the layer structure fabricated from carbon and polytetrafluoroethylene (PTFE). PTFE is not only providing the hydrophobic property, but it is melted to be the binder for welding carbon particles and forming the film by sintering method. The porosity in the film is achieved by mixing PTFE and carbon with sugar. During sintering, sugar decomposes producing bubbles and then increasing the porosity. As for the effect of the surrounding environment, too low or high humidity may lead to drying-out of electrolyte or flooding of the air electrode. GDL side also prevents the water leakage from the battery. The electrode conductivity can be increased with carbon ratio. As a result, GDL has to be balanced the hydrophobicity and conductivity. Well balance of its properties can help slow down water evaporation loss or resist flooding. The suitable ratio is about 25-60% PTFE depending on their level of material properties (Bidault, Brett et al. 2009). GDL is usually coated on porous current collecting materials especially nickel or carbon and has to be as thin as possible in order to maximize oxygen gas permeability. The PTFE-bonded layer works efficiency for aqueous electrolytes. On the other hand, it is not suitable for aprotic or ionic liquid electrolyte, as mention in section 2.1.3, because PTFE and carbon electrode pores can be flooded and pushed out the gas by organic solvents (Li and Dai 2014).
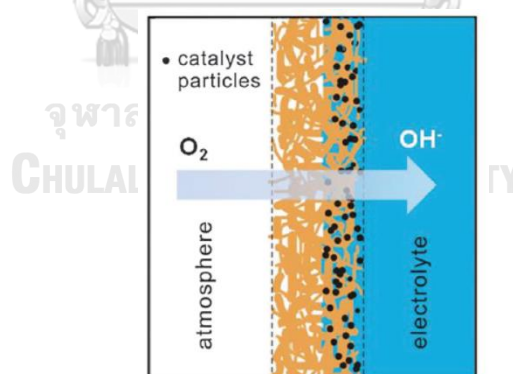
Figure 2.1 The structure of gas diffusion electrode (Li and Dai 2014)

The reaction kinetics of ORR is slow, so it requires catalyst for bond activation breaking strong O=O bond. Many researches introduced electrocatalysts to reduce ORR overpotential such as silver, metal oxides (i.e. MnO_2, Co_3O_4) or perovskite oxides ($La_{0.6}Ca_{0.4}CoO_3$). In general, MnO_2 is the most common ORR catalyst in commercial zinc-air batteries. For rechargeable batteries, the air electrode should be effective both ORR and OER so bifunctional catalysts have to be used. The air electrode usually degrades within a few numbers of cycle during ORR-OER cycle.

Because OER generates the bubble gas that will damage the structure on the air electrode and the alternation of reductive and oxidative environments may cause unrecoverable damage to the catalyst (Li and Dai 2014). One way to avoid electrocatalytic limitation is three-electrode configuration describing later in section 2.3.2.

2.2 Principle of zinc-air battery

The electrochemical reaction transfers the charge between the electrode and chemical species. The rate of charge producing from the reaction is current. The electron energy of each reaction is measured in potential. Zinc-air batteries have a standard potential of 1.6 V which calculated from equation 2.3. E^0 cell is the potential at equilibrium which the net current flow equal to zero. In practice, the potential while discharge is about 1.2 V or lower. And the voltage while charge is about 2 V or higher. They result from the overpotential required to drive the passage of current through the resistance. Because of this, roundtrip energy efficiency is low about 60%.

$$E^0{}_{Cell} = E^0{}_{Cathode} - E^0{}_{Anode} \qquad (2.3)$$

2.2.1 Discharging process
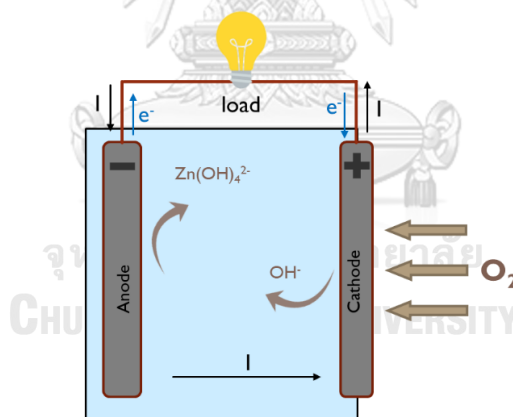
Figure 2.2 The transfer direction of electron and current during discharging process

The zinc-air battery uses oxygen in the surrounding air to be the reactant. Oxygen diffusing through the GDL at the air electrode is reduced with catalyst on the catalytic layer and water in the electrolyte. The reaction 1.1 and 1.2 occur at the surface of both electrodes. ORR produces hydroxide to the electrolyte. Zinc is oxidized with hydroxide in the electrolyte at zinc-electrode giving electrons for ORR reaction. The zinc oxidation produces zincate ion $(Zn(OH)_4{}^{2-})$. After they are supersaturated, zincate ion decomposes to insoluble zinc oxide (reaction 1.3). This zinc oxide will block the active zinc surface creating passivation. Moreover, parasitic electrochemical reaction (1.6) also arises at the zinc electrode. It consumes zinc,

water, and hydroxide in the electrolyte. This reaction leads to corrosion on the zinc electrode and it will be discussed in section 2.3.1.

Cathode: $\frac{1}{2}O_2 + H_2O + 2e^- \rightarrow 2OH^-$ $E^0 = 0.4$ V   (1.1)

Anode: $Zn + 4OH^- \rightarrow Zn(OH)_4{}^{2-} + 2e^-$ $E^0 = -1.2$ V   (1.2)

$Zn(OH)_4{}^{-2} \rightarrow ZnO + 2OH^- + H_2O$ (1.3)

Overall: $2Zn + O_2 \rightarrow 2ZnO$ $E^0{}_{cell} = 1.6$ V   (1.4)

Parasitic reaction: $Zn + 2OH^- + 2H_2O \rightarrow Zn(OH)_4{}^{-2} + H_2$ (1.6)
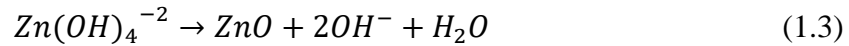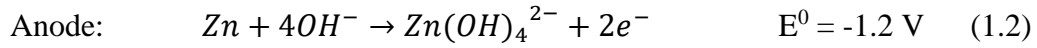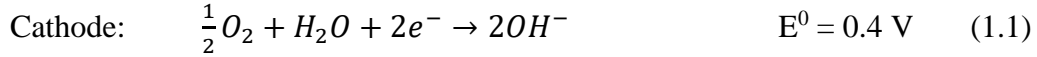
2.2.2 Charging process
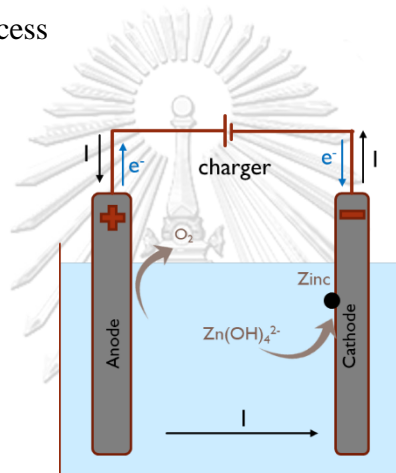
Figure 2.3 The transfer direction of electron and current during charging process

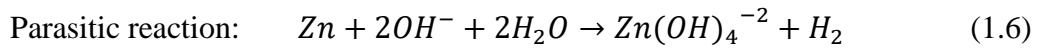The charging process as mentioned in section 1.1, the reactions are reversed as showed below. According to overall reaction, zinc metals are plated on the electrode and oxygen is generated at anode. Since the zincs are not formed at the same place that they dissolve, shape changes and dendritic growth takes place at the electrode. Apart from this, oxygen evolution will damage the electrode. The problem and solution of this has discussed in section 2.3.2.

Anode : $2OH^- \rightarrow \frac{1}{2}O_2 + H_2O + 2e^-$ $E^0 = 0.4$ V   (2.4)

Cathode: $Zn(OH)_4{}^{2-} + 2e^- \rightarrow Zn + 4OH^-$ $E^0 = -1.2$ V   (2.5)

Overall: $2ZnO \rightarrow 2Zn + O_2$ $E^0{}_{cell} = 1.6$ V   (2.6)

HER: $2H_2O + 2e^- \rightarrow H_2 + 2OH^-$ $E^0 = -0.8$ V   (1.5)
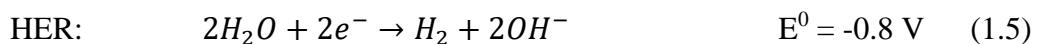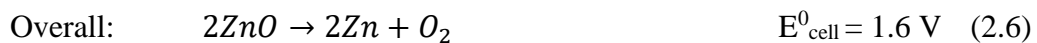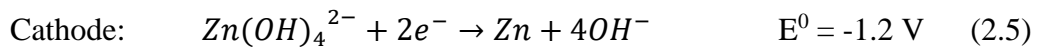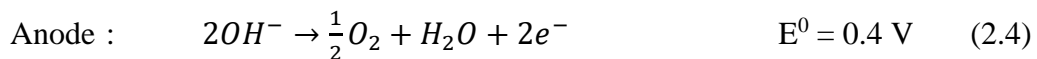
2.3 Problem and solution

2.3.1 Hydrogen evolution reaction

$$Zn + 4OH^- \leftrightarrow Zn(OH)_4{}^{2-} + 2e^- \qquad \text{E}^0 = \text{-1.2 V} \qquad (1.2)$$

$$2H_2O + 2e^- \rightarrow H_2 + 2OH^- \qquad \text{E}^0 = \text{-0.8 V} \qquad (1.5)$$
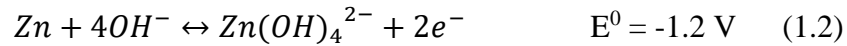
For the charging process, zincate is reduced to zinc metal. The rise of hydrogen on the zinc electrode is unavoidable. Due to the HER is thermodynamically preferred, as the value of its standard reduction potential is higher than zinc reduction. Therefore, the coulombic efficiency of the zinc electrode will be lowered by the presented of the HER (Dundálek, Šnajdr et al. 2017). For the discharging process, some of electron from zinc dissolution reaction is caught by water and then hydrogen rising instead of current producing. Therefore, the effective electron for the discharging process is decreased by HER.

2.3.2 Three-electrode configuration

The way to avoid degradation of the air electrode is three-electrode configuration to improve the cycle-life of the battery as mentioned above. Two air electrodes are employed one for charge and another for discharge. The zinc electrode is placed between them and connected to the air electrode or ORR electrode for discharge and changed to the third electrode or OER electrode for charge. From previous researches, the OER electrode materials mostly different from the ORR electrode such as Ag$_2$O and LaNiO$_3$ or only stainless steel but sometimes same as the ORR electrode. Furthermore, the addition of the third electrode increases the volume of battery and decreases volumetric power density. However, this configuration easy to manipulate for better performance (Li and Dai 2014). Hong (2016) introduced a horizontal three-electrode structure which evaluated cycle life by charge-discharge cycle test with 1000 cycles at 20 mA/cm^2. The average columbic efficiency and energy efficiency are 90% and 42%, respectively.
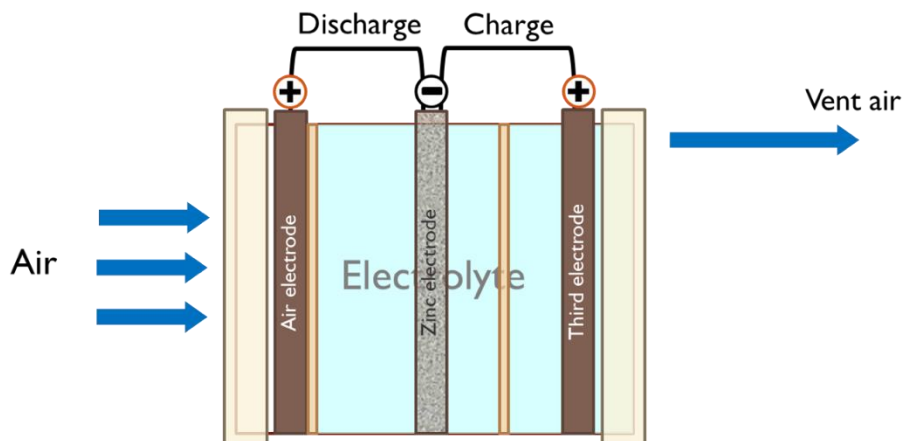

Figure 2.4 The structure of three-electrode zinc air battery in plate form

2.3.3 Shunt current

The shunt currents occur when the flow cells system electrically connected in series. As the electrolyte has high conductivity, electrolyte connections offer additional current paths between all battery cells (Wandschneider, Röhm et al. 2014). During charge, since the leaked current flow through the manifold, the current flowing through the cell is lower than the current input. On the other hand, while discharge, the current discharging in each cell increased by shunt currents. Therefore, some of energy loss by shunt currents.

Amunátegui et al. introduced an integrated battery in pilot-scale with 4 kWh. They studied the shunt currents phenomenon which occurs when the electrolyte flow system connected. It reduced coulombic efficiency by 18%. This phenomenon effect is evaluated by mathematical model. (Amunátegui, Ibáñez et al. 2018)

2.4 Mathematical model

2.4.1 Literature reviews of Zinc-Air battery (ZAB) modeling

Table 2.1 The review of Zinc-Air battery (ZAB) modeling literature

Reference	Topic	Detail
(Amunátegui, Ibáñez et al. 2018)	Electrochemical energy storage for renewable energy integration: zinc-air flow batteries	The pilot plant of 4 kWh design specification was built. The one stack of 20-cells connected in series was picked to study the shunt currents phenomenon by mathematical model. The results showed that the coulombic efficiency was lower than expected due to the shunt currents loss.
(Deiss, Holzer et al. 2002)	Modeling of an electrically rechargeable alkaline Zn-air battery	One-dimensional modeling of rechargeable ZAB with static electrolyte based on dilute solution theory. The HER was considered. The cell voltage of both electrodes was calculated. And, the concentration profile was indicted. It showed that the redistribution of Zn and ZnO (shape change) decrease with increasing cycle number.
(Dundálek, Šnajdr et al. 2017)	Zinc electrodeposition from flowing alkaline zincate solution: Role of HER	This work focusses on the zinc electrode which zinc deposit reaction and HER occur. The model evaluated the effect of hydrogen bubble rising on the convection within the diffusion layer.
(Jung, Kim et al. 2016)	Computational analysis of the zinc utilization in the primary zinc-air batteries	A one-dimension of discharging zinc-air battery is implemented. The model based on the concentrate solution theory. This work aims to study the effect of OH ion on the formation of ZnO. And, the performance is predicted by varying the thickness of anode and separator. It found that more compact anode is favored to improve zinc utilization.

(Lao-atiman, Bumroongsil et al. 2019)	Model-based analysis of an integrated Zinc-air flow battery/ Zinc electrolyzer system	A zinc-air flow battery integrated with the zinc electrolyzer had introduced. The zero-dimension model is used to study the effect of electrolyte flow rate, electrolyte concentration. This model involved the effect of HER which decrease the coulombic efficiency. The result shows that optimal KOH is about 6 to 7M. High initial ZnO can decrease HER. And, high electrolyte flow rate can enhance the battery performance.
(Schröder and Krewer 2014)	Model based quantification of air-composition impact on secondary zinc air batteries	The isothermal zero-dimension model was developed to analyze the impact of air composition with humidity, CO_2 and O_2 content. The results showed that pure O_2 at appropriate humidity and avoiding CO_2 impurity was favorable to operate the zinc air battery.
(Wandschneider, Röhm et al. 2014)	A multi-stack simulation of shunt currents in vanadium redox flow batteries	A model for the shunt currents in an all-vanadium redox flow battery was developed. The pipe connections between the stacks give rise to external shunt currents leading to a nonuniform distribution of current.

2.4.2 Principle of electrochemistry

Electrochemical cell is classified as either galvanic cells or electrolytic cells. *The galvanic cells* are one which faradaic reactions occur spontaneously at the electrodes connected externally by loads. The faradaic reactions are the electrochemical reactions that involve charge transfer. The reactions convert chemical energy into electrical energy by transferring of electron and ion. *The electrolytic cells* are one which the reactions occur in the opposite direction. The reactions are driven by external voltage greater than open-circuit potential of the cell which inputs electrical energy to be stored as chemical energy. In electrochemical cells, an oxidation reaction occurs at the anode that producing electron. Whereas, a reduction reaction occurs at the cathode that consuming electron on the electrode. For the galvanic cells, the cathode is positive with respect to the anode. In contrast, for the electrolytic cells, the cathode is negative with respect to the anode. In the half-cell aspect, a current which electron crosses the interface from the electrode to a species in the solution is cathodic current. While the current which electron flow from solution species to the electrode is anodic current.

2.4.2.1 Charge transfer

The current (I) represents the number of electrons reacting per second or the number of electric charges (Q) flowing per second. So, the current is a direct method to measure the electrochemical reaction rate. From Faraday's law, the rate of charge transfer is

$$I = \frac{dQ}{dt} \tag{2.7}$$

$$\frac{dN}{dt} = \frac{I}{nF} \tag{2.8}$$

where dN/dt is the electrochemical reaction rate, n is the number of charge transfer in the reaction, and F is Faraday's constant (96,485 coulomb/mol). These reactions occurring at the electrode surface are the heterogeneous reaction. The reactions depend on the area of the electrode. Therefore, rate of reactions is usually described in units of mol per second per area or current density (i).

$$Rate = \frac{I}{nFA} = \frac{i}{nF} \tag{2.9}$$

2.4.2.2 Charge transfer reactions

The electrochemical reaction in reduction form is below where O is oxidized species and R is reduced species.

$$O + ne \leftrightarrow R \tag{2.10}$$

When the potential is more negative than equilibrium potential. It will create more R. In contrast, when the potential is more positive than equilibrium potential. It will create more O.

The net current generating or consuming is

$$\frac{i}{nF} = k_f C_O - k_b C_R \tag{2.11}$$

C_o and C_R are the concentration of O and R. The rate coefficient (k) which k_f for forward reaction and k_f for backward reaction is calculated by electrode kinetic.

$$k = k_0 exp\left(-\alpha\frac{F}{RT}(E - E_0)\right) \tag{2.12}$$

where k_0 is standard rate constant, α is the transfer coefficient of the reaction, E is the potential, and E_0 is standard electrode potential.

$$i = nF\left[k_{0,f}C_O exp\left(\frac{-\alpha F(E-E_0)}{RT}\right) - k_{0,b}C_R exp\left(\frac{(1-\alpha)F(E-E_0)}{RT}\right)\right] \tag{2.13}$$

These reactions are reversible. The exchange current density (i_0) is the rate at equilibrium state. The net current is zero. From equation 2.12, i_0 can be expressed by

$$i_0 = nFk_{0,f}C_O exp\left[\frac{-\alpha_{Rd}F(E_{eq}-E_0)}{RT}\right] = nFk_{0,b}C_R exp\left[\frac{-\alpha_{Ox}F(E_{eq}-E_0)}{RT}\right] (2.14)$$

For low current density or no-mass transfer effect, the net rate can be calculated by the Butler-Volmer equation:

$$i = i_0\left[exp\left(\frac{\alpha nF}{RT}\cdot\eta_{act}\right) - exp\left(\frac{-(1-\alpha)nF}{RT}\cdot\eta_{act}\right)\right] \qquad (2.15)$$

At the high currents, the surface concentrations have to be considered the difference between bulk and surface, the Butler-Volmer equation or sometimes called the current-overpotential becomes:

$$i = i_0\left[\left(\frac{C_{O,s}}{C_{O,b}}\right)exp\left(\frac{\alpha nF}{RT}\cdot\eta_{act}\right) - \left(\frac{C_{R,s}}{C_{R,b}}\right)exp\left(\frac{-(1-\alpha)nF}{RT}\cdot\eta_{act}\right)\right] \quad (2.16)$$

Where

$$\eta_{act} = E - E_{eq} \qquad (2.17)$$

2.4.2.3 Transport processes in electrolyte solution

Applying potential across an ionic solution produces a driving force for ionic current. Mass transfer arises from the differences in electrical or chemical potential or from the movement of a volume of the solution. It can occur due to:

- Migration is the movement of charge due to a potential gradient.
- Diffusion is the movement of species due to a concentration gradient.
- Convection is the result of forces on the solution such as the velocity of bulk fluid or volume change of the system.

$$J_k = J_k^{dif} + J_k^{mig} + J_k^{con} \qquad (2.18)$$

Three types of transport processes are combined to be The Nernst-Planck equation. For low ionic strength electrolyte, a dilute solution theory (DST) approach can be applied to the model (Clark, Latz et al. 2018). In DST, the interaction of a solute species with other solutes are neglected. Each species diffuses independently due to its concentration gradient and diffusion coefficient.

$$J_k = -D_k\nabla C_k - \frac{z_k F}{RT}D_k C_k\nabla\phi + C_k v \qquad (2.19)$$

For high ionic strength electrolyte, a concentrate solution theory (CST) is needed. In CST, the interaction among all species present in the solution.

$$J_k = -D_k\nabla C_k - \frac{t_k}{z_k F}\cdot i + C_k v \qquad (2.20)$$

where t_k is transference number of ion k determined by properties of all present ion which calculated from the equation below, z_k is charge number of species k, and F is Faraday constant (Schröder and Krewer 2014).

$$t_k = \frac{z_k^2 \cdot \frac{D_k F}{RT} \cdot \tilde{C}_k}{\sum_n z_n^2 \cdot \frac{D_n F}{RT} \cdot \tilde{C}_n} \tag{2.21}$$

$$\tilde{C}_k = \frac{C_k^{air} + C_{k,b}}{2} \tag{2.22}$$

2.4.2.4 Electrical double layer

At the metal-solution interface, the excess of charge on the electrode surface is counterbalanced by the accumulation of ions with the opposite charge in the solution. This charge separation is called the electrical double layer. The Helmholtz model describes the double layer as a parallel plate capacitor which the potential changes linearly from electrode potential to electrolyte potential crossing the small thickness. This layer is referred to as the Helmholtz layer and can be described by a constant capacitance (C_{dl}).

$$Q = C_{dl} E_c \tag{2.23}$$

where E_c is the voltage across the capacitance.

At the beginning of the charging process, most of total current is used for charging the double layer until charge (Q) satisfies. Thus, the current for charge transfer reactions is very small. However, when double layer is fully charge, the total current will be used for the reactions.

2.4.2.5 Potential

For electrochemistry, Nernst equation provides a linkage between electrode potential and the concentration participants in the electrode process.

$$E = E_0 + \frac{RT}{nF} ln \frac{C_O}{C_R} \tag{2.24}$$

The electrode reaction must be thermodynamically or electrochemically reversible (Nernstian).

2.4.2.6 Equivalent circuit

An equivalent circuit model is used to represent an electrochemical cell as following:
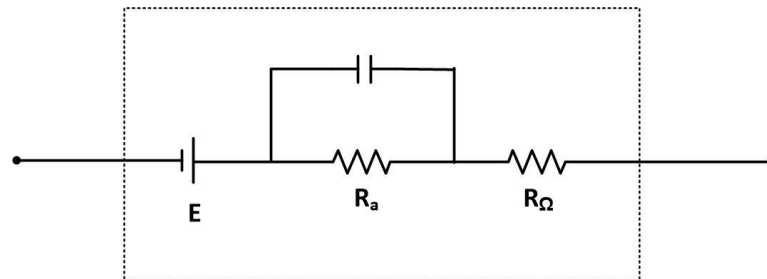
Figure 2.5 Equivalent circuit of electrochemical cell

R_Ω represents the ohmic loss in the battery which includes the resistance of electrodes interface and the resistance through the electrolyte. R_a is activation loss. The electrical double layer is represented by capacitor in this circuit.

2.4.3 Model description

Reaction A: $\frac{1}{2}O_2 + H_2O + 2e^- \leftrightarrow 2OH^-$ (1.1)

Reaction B: $Zn + 4OH^- \leftrightarrow Zn(OH)_4{}^{2-} + 2e^-$ (1.2)

Reaction C: $2H_2O + 2e^- \rightarrow H_2 + 2OH^-$ (1.5)

Reaction D: $Zn(OH)_4{}^{-2} \leftrightarrow ZnO + 2OH^- + H_2O$ (1.3)

Figure 2.6 Schematic view of the model regions

2.4.3.1 Material balance in the zinc electrode

For the dissolved species k in the electrolyte: OH⁻, $Zn(OH)_4^{-2}$ and H_2O, the material balance equation has to be solved to yield the time-dependent concentration profile. This equation for the bulk electrolyte (Fig.2.6) is given by

$$\frac{d(C_{k,b}V_e{}^{zn})}{dt} = F_{k,in} - F_{k,out} + J_k + j_k^{dif,S} + \sum_r R_k^r \quad (2.25)$$

where $C_{k,b}$ is the concentration of species k in the bulk electrolyte, V_e is the electrolyte volume, $F_{k,in}$ and $F_{k,out}$ are the molar flow rate of species k in and out the bulk electrolyte, J_k is rate of molar transfer across the electrode of species (Equation 2.17), $j_k^{dif,S}$ is rate of diffusion transfer of species k from the bulk electrolyte to diffusion layer on the zinc electrode surface, and R_k^r is the reaction rate of production or consumption of species k in reaction r.
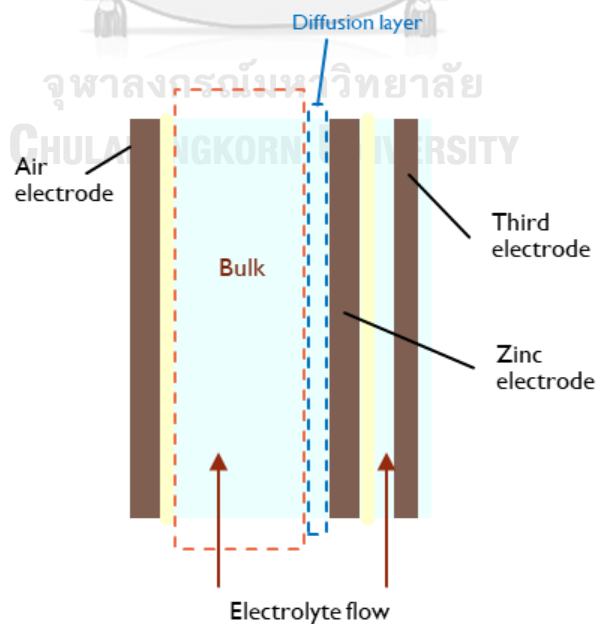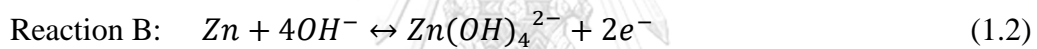
$$\frac{dC_{k,b}}{dt} = \frac{1}{V_e{}^{zn}}\left[F_{k,in} - F_{k,out} + J_k + j_k^{dif,S} + \sum_r v_k^r R_k^r\right] \quad (2.26)$$

The molar flow rate equation is below where the v is the volumetric flow rate of the electrolyte.

$$F_k = C_{k,b} \cdot v \quad (2.27)$$

Material balance in the air electrode ($C_{k,a}$) is expressed by:

$$\frac{dC_{k,a}}{dt} = \frac{1}{V_e{}^{air}}\left[-J_k + \sum_r v_k^r R_k^r\right] \quad (2.28)$$

Material balance in the diffusion layer on the electrode surface ($C_{k,s}$) is expressed by:

$$\frac{dC_{k,s}}{dt} = \frac{1}{\delta_{k,dif} \cdot A_{zn}}\left[-j_k^{dif,S} + \sum_r v_k^r R_k^r\right] \quad (2.29)$$

The volume of this layer is assumed to be constant with time. A_{zn} is the area of zinc electrode, and $\delta_{k,dif}$ is the thickness of diffusion layer.

The electroneutrality condition for ion species in the solution must be concerned.

$$\sum_k z_k C_{k,b} = 0 \quad (2.30)$$

For the solid species: ZnO, the material balance is given by

$$\frac{d(N_{ZnO})}{dt} = R_{ZnO} \quad (2.31)$$

According to the assumption, described in section 3.1, ZnO reaction occurs at the bulk of electrolyte. And for Zn-metal

$$\frac{d(N_{Zn})}{dt} = -R_{Zn} \quad (2.32)$$

where N_{ZnO} and N_{Zn} are the molar of species ZnO and Zn

2.4.3.2 Molar transfer of dissolved species in the electrolyte

Molar transfers include diffusion, migration, and convection are the driving force of species in the electrolyte for transference ion between both electrodes. Convection transfer in this model is neglected.

$$J_k = J_k^{dif} + J_k^{mig} \tag{2.33}$$

where J_k^{dif} is the molar transfer of species k given by

$$J_k^{dif} = D_k \frac{C_{k,a} - C_{k,b}}{\delta_{sep}} \cdot \varepsilon_{sep} \cdot A_{sep} \tag{2.34}$$

D_k is the diffusion coefficient of species k, $C_{k,a}$ is the concentration of species k in the air electrode, and δ_{sep}, ε_{sep} and A_{sep} are the properties of separator which are thickness, porosity and area, respectively. The migration transfer of species k, J_k^{mig}, for CST given by

$$J_k^{mig} = \frac{t_k}{z_k F} \cdot i^{cell} \cdot \varepsilon_{sep} \cdot A_{sep} \tag{2.35}$$

t_k is calculated by equation 2.20 and 2.21 as mention in section 2.4.2.3. In the same way, rate of diffusion transfer between bulk and surface can be expressed as

$$j_k^{dif,s} = D_k \frac{C_{k,s} - C_{k,b}}{\delta_{k,dif}} \cdot A_{zn} \tag{2.36}$$

2.4.3.3 Diffusion layer

Diffusion layers occur on the interface between the electrode surface and electrolyte solution where reactant species diffuse from the solution to react on the surface and product species diffuse out of the surface. The thickness of diffusion layer is calculated by Sherwood number (Sh) as follow (Dundálek, Šnajdr et al. 2017):

$$\delta_{k,dif} = \frac{d_{eq}}{Sh} \tag{2.37}$$

$$Sh = 1.85 \left(\frac{d_{eq}}{l} \cdot Re \cdot Sc \right)^{\frac{1}{3}} \tag{2.38}$$

$$Re = \frac{d_{eq} v \rho}{\mu} \tag{2.39}$$

$$Sc = \frac{\mu}{D_k \rho} \tag{2.40}$$

Where l is the length of the electrode, Re is Reynold number, Sc is Schmidt number, v, ρ and μ is velocity, density and viscosity of bulk electrolyte, and d_{eq} is hydraulic diameter, for annulus, which calculated by:

$$d_{eq} = \frac{4 \cdot \frac{\pi (d_{out}^2 - d_{in}^2)}{4}}{\mu (d_{out} - d_{in})} = d_{out} - d_{in} \tag{2.41}$$

2.4.3.4 Rate of reactions

The electrochemical reaction rates in equations as following arise from reactions A, B, C and D. These reactions occur on the electrode surface. In the equation (2.45-2.56), i_{air}, i_{zn} and i_H are current density which consumed or produced by the reaction A, B and C, respectively, multiplies with the area which reactions occur (A_{zn} is area of air electrode).

$$R_A = \frac{i_{air} \cdot A_{air}}{nF} \tag{2.42}$$

$$R_B = \frac{i_{zn} \cdot A_{zn}}{nF} \tag{2.43}$$

$$R_C = \frac{i_H \cdot A_{zn}}{nF} \tag{2.44}$$

The charge transfer (i_{air}, i_{zn} and i_H) is described with a Butler-Volmer approach as described in section 2.4.2.2 presented by:

For discharge

$$i_{air} = i_0^{air} \left[\left(\frac{C_{O_2,s}}{C_{O_2,atm}} \right)^{\frac{1}{2}} exp \left(\frac{\alpha_{air} nF}{RT} \eta_{act}^{air} \right) - \left(\frac{C_{OH^-,a}}{C_{OH^-,b}} \right)^2 exp \left(\frac{-(1-\alpha_{air})nF}{RT} \eta_{act}^{air} \right) \right] \tag{2.45}$$

$$i_0^{air} = a_c \delta_{active} i_0^{air.ref} \tag{2.46}$$

$$\frac{dC_{O_2,s}}{dt} = \frac{1}{V_e^{air}} \left[-0.5 \cdot R_A - D_{O_2,air} \frac{C_{O_2,s} - C_{O_2,atm}}{\delta_{GDL} A_{air}} \right] \tag{2.47}$$

For charge

$$i_{air} = i_0^{air} \left[\left(\frac{C_{O_2,s}}{C_{O_2,ref}} \right)^{\frac{1}{2}} exp \left(\frac{\alpha_{air} nF}{RT} \eta_{act}^{air} \right) - \left(\frac{C_{OH^-,a}}{C_{OH^-,b}} \right)^2 exp \left(\frac{-(1-\alpha_{air})nF}{RT} \eta_{act}^{air} \right) \right] \tag{2.48}$$

$$i_0^{air} = a_c \delta_{filmair} i_0^{air.ref} \tag{2.49}$$

$$\frac{dC_{O_2,s}}{dt} = \frac{1}{V_e^{rd}} \left[-0.5 \cdot R_A - D_{O_2,KOH} \frac{C_{O_2,s} - C_{O_2,ref}}{\delta_{rd} A_{air}} \right] \tag{2.50}$$

where a_c is the effective area, δ_{active} and $\delta_{filmair}$ are reaction zone thickness. The concentration of dissolved oxygen in the air electrode is given by (Schröder and Krewer 2014) as shown in above.

The charge transfer of zinc is presented by:

$$i_{zn} = i_0^{zn} \left[\left(\frac{C_{OH^-,s}}{C_{OH^-,b}} \right)^4 exp \left(\frac{\alpha_{zn} nF}{RT} \eta_{act}^{zn} \right) - \left(\frac{C_{Zn(OH)_4^{2-},s}}{C_{Zn(OH)_4^{2-},b}} \right) exp \left(\frac{-(1-\alpha_{zn})nF}{RT} \eta_{act}^{zn} \right) \right] \tag{2.51}$$

$$i_0^{zn} = a_s X_{zn} i_0^{zn,ref} \tag{2.52}$$

$$a_s = a_0 \left(\frac{1-\varepsilon}{1-\varepsilon_0} \right)^{2/3} \tag{2.53}$$

$$X_{zn} = \frac{(N_{zn} \cdot \bar{V}_{zn})^{2/3}}{(N_{zn} \cdot \bar{V}_{zn})^{2/3} + (N_{ZnO} \cdot \bar{V}_{ZnO})^{2/3}} \tag{2.54}$$

where a_s is solid-solution interface area per unit volume (Jung, Kim et al. 2016), a_0 is initial solid-solution interface area per unit volume, ε is the porosity of zinc electrode, X_{zn} is the factor which accounts for the rate reaction that proportional to the surface of zinc particle within the electrode, and where δ_{zn} is zinc electrode thickness. The HER described in reaction C is neglected the reverse reaction given by (Dundálek, Šnajdr et al. 2017)

$$i_H = i_0^H \left[-exp\left(\frac{-(\alpha_H)nF}{RT} \eta_H \right) \right] \tag{2.55}$$

$$i_0^H = a_s X_{zn} i_0^{H,ref} \tag{2.56}$$

The chemical reaction rate is zinc oxide precipitation that occurs in the electrolyte.

$$R_D = k_s \left(C_{Zn(OH)_4^{2-}} - C_{Zn(OH)_4^{2-},sat} \right) \tag{2.57}$$

where k_s is rate constant, and $C_{Zn(OH)_4^{2-},sat}$ is the concentration of zincate at saturation limit. This reaction will occur when the zincate concentration is greater than $4 \cdot C_{Zn(OH)_4^{2-},sat}$ as mention in Stamm, Varzi et al. (2017).

2.4.3.5 Volume change

The volume of solid on the electrode changing with time is given by

$$\frac{dV_{solid}}{dt} = \frac{d(N_{Zn})}{dt} \cdot \bar{V}_{zn} + \frac{d(N_{ZnO})}{dt} \cdot \bar{V}_{ZnO} \tag{2.58}$$

$$\varepsilon = 1 - \frac{V_{solid}}{\delta_{zn} A_{zn}} - (1 - \varepsilon_0) \tag{2.59}$$

The porosity of zinc electrode, ε, is changed by the volume change of solid.

2.4.3.6 Cell potential

The cell potential (E_{cell}) is calculated from the potential of each electrode minus with overpotential which consists of activation loss and ohmic loss.

$$E_{cell} = E^{air} - E^{zn} - \eta_{act}^{zn} - \eta_{act}^{air} - \eta_{ohm} \tag{2.60}$$

E^{air} is the potential at the air electrode and E^{zn} is the potential at the zinc electrode. They are calculated from Nernst equation which depends on concentration at the electrode surface.

$$E^{air} = E_0^{air} + \frac{RT}{nF} ln\left(\frac{(C_{O_2}/C^{ref})^{0.5}}{(C_{OH^-}^{air}/C^{ref})^2} \right) \tag{2.61}$$

$$E^{zn} = E_0^{zn} + \frac{RT}{nF} ln \left(\frac{\left(C_{Zn(OH)_4^{2-},s}/C^{ref} \right)}{\left(C_{OH^-,s}/C^{ref} \right)^4} \right) \tag{2.62}$$

where E_0^{air} is the standard potential of air electrode, E_0^{zn} is the standard potential of zinc electrode, and C^{ref} is the concentration at reference state. According to side reaction occurred at zinc electrode, E^H is the potential of HER. And, E_0^H is the standard potential of HER.

$$E^H = E_0^H - \frac{RT}{nF} ln \left(\frac{C_{OH^-,s}}{C^{ref}} \right) \tag{2.63}$$

$$\Delta E_{ZH} = E^{zn} - E^H \tag{2.64}$$

$$\eta_H = \eta_{act}^{zn} + \Delta E_{ZH} \tag{2.65}$$

2.4.3.7 Charge balances

Each electrode is described with equations account for transient changes of the electrode overpotential that is activation loss. The activation loss occurring at the zinc electrode (η_{act}^{zn}) is calculated by current density from zinc dissolution (i_{zn}) and HER (i_H). C_{dl}^{zn} is double layer capacitance of the zinc electrode as well as the air electrode. (Schröder and Krewer 2014)

$$\frac{d\eta_{act}^{zn}}{dt} \cdot C_{dl}^{zn} = i_{cell} - (i_{zn} + i_H) \tag{2.66}$$

$$\frac{d\eta_{act}^{air}}{dt} \cdot C_{dl}^{air} = i_{cell} - i_{air} \tag{2.67}$$

2.4.3.8 Ohmic loss

Ohmic potential loss (η_{ohm}) is only accounted for due to ion transport resistance and resistance at zinc electrode and air electrode (Schröder and Krewer 2014). The applied ohmic potential loss with:

$$\eta_{ohm} = i_{cell} \cdot A_{cell} \cdot R_{ohm} \tag{2.68}$$

$$R_{ohm} = \frac{\delta_{zn}}{\sigma_{electrode}^{zn} \cdot A_{zn}} + \frac{\delta_{elec}}{\sigma_{elec} \cdot A_{elec}} + \frac{\delta_{GDL}}{\sigma_{electrode}^{air} \cdot A_{air}} + R_{comp} \frac{\delta_{comp}}{A_{cell}} \tag{2.69}$$

where A_{cell} is area of cell, $\sigma_{electrode}^{zn}$, σ_{elec} and $\sigma_{electrode}^{air}$ are the conductivity of zinc electrode, electrolyte and air electrode, respectively, δ_{elec} is the thickness of electrolyte channel, R_{comp} is the resistance of component of the battery and δ_{comp} is component thickness. The conductivity of zinc electrode is calculated by

$$\sigma_{electrode}^{zn} = \left(\frac{N_{zn} \cdot \bar{V}_{zn}}{\delta_{zn} \cdot A_{zn}} \right) \cdot \sigma_{zn} + \sigma_{Ni} \cdot (1 - \varepsilon) \tag{2.70}$$

where σ_{zn} is conductivity of zinc metal and σ_{Ni} is conductivity of nickel.

2.4.3.9 Shunt current model

The figure below represents the electrolyte flow paths between battery cells. Each pathway has a small resistance (R) of electrolyte. The subscript b is branch path and m is main path. Also, the additional subscript c is cathode side and a is anode side.
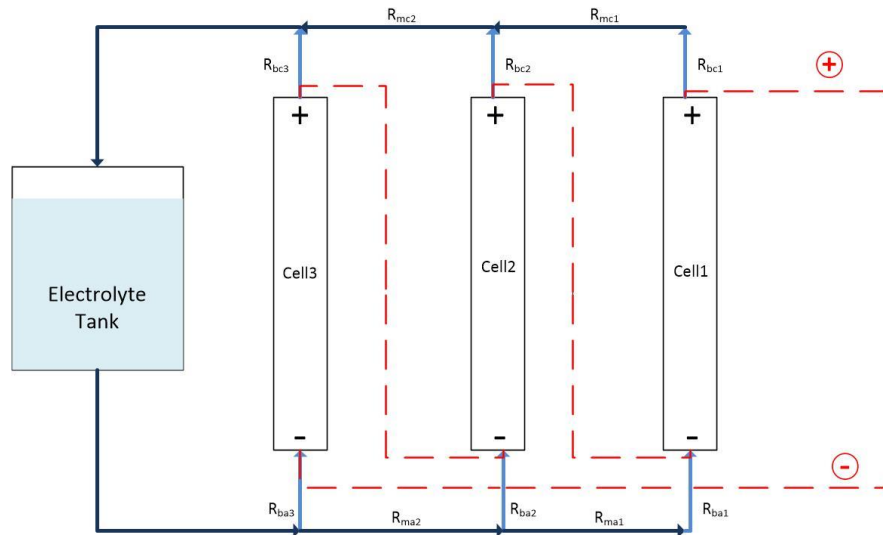

Figure 2.7 Battery flow paths between 3-cells battery connected in series

The shunt current equivalent electric circuit is shown below. The current flow through the cell and separate through the electrolyte paths. The set of equations is obtained by applying Kirchoff's Laws at every node and mesh.
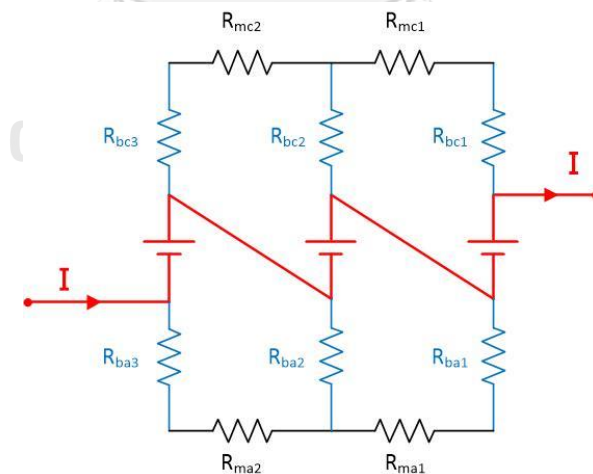

Figure 2.8 The shunt currents equivalent electric circuit with electrolyte resistance
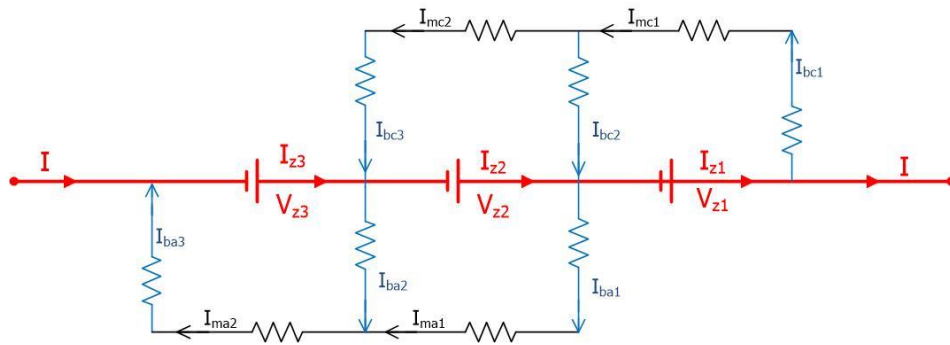
Figure 2.9 The shunt currents in rearranged equivalent electric circuit with current direction

From Kirchoff's Current Law: The case with n wires all connected at a node can be expressed:

$$\sum_n I_n = 0 \tag{2.71}$$

There are 6 nodes in the circuit. So, it is expressed by

$$I_{z1} = I + I_{bc1}$$

$$I_{z1} + I_{ba1} = I_{z2} + I_{bc2}$$

$$I_{z2} = I_{z3} + I_{bc3} + I_{bc2}$$

$$I_{z3} = I_{ba3} + I$$

$$I_{bc1} = I_{bc2} + I_{bc3}$$

$$I_{ba1} = -I_{ba2} + I_{ba3}$$

From Kirchoff's Voltage Law: The sum of all potential differences across the component involved in each loop must be zero.

$$\sum_n V_n = 0 \tag{2.72}$$

There are 4 loops in the circuit. So, the equations are obtained:

$$V_1 = I_{bc1}(R_{bc1}) + I_{mc1}(R_{mc1}) + I_{bc2}(R_{bc2})$$

$$V_2 = -I_{bc2}(R_{bc2}) + I_{bc3}(R_{bc3}) + I_{mc2}(R_{mc2})$$

$$V_2 = I_{ba1}(R_{ba1}) + I_{ma1}(R_{ma1}) - I_{ba2}(R_{ba2})$$

$$V_3 = I_{ba2}(R_{ba2}) + I_{ba3}(R_{ba3}) + I_{ma2}(R_{ma2})$$

Some rearrangement has been done on these equations for the 3-cells example. In the assumption of R_b and R_m at all positions are constant at same value. And, the currents passing same path have same value (e.g. $I_{bc1} = I_{mc1}$). We obtain that

$$I_{bc2} = \frac{V_{z1} - V_{z2}}{3 \cdot R_b + R_m}$$

$$I_{bc3} = \frac{V_{z2} + I_{bc2} \cdot R_b}{R_b + R_m}$$

$$I_{bc1} = I_{bc2} + I_{bc3}$$

$$I_{ba2} = \frac{V_{z3} - V_{z2}}{3 \cdot R_b + R_m}$$

$$I_{ba3} = \frac{V_{z3} + I_{ba2} \cdot R_b}{R_b + R_m}$$

$$I_{ba1} = -I_{ba2} + I_{ba3}$$

$$I_{z1} = I_{bc1} + I$$

$$I_{z2} = I_{z1} + I_{ba1} - I_{bc2}$$

$$I_{z3} = I_{z2} - I_{bc3} + I_{ba2}$$

The resistance of electrolyte flow path calculated from equation below.

$$R_m = \frac{L_m}{\sigma_{elec} \cdot A_{elecTube}} \qquad (2.73)$$

$$R_b = \frac{L_b}{\sigma_{elec} \cdot A_{elecTube}} \qquad (2.74)$$

In addition, this work also demonstrates the stack of 2, 4 and 5 cells. The calculation is showed below.
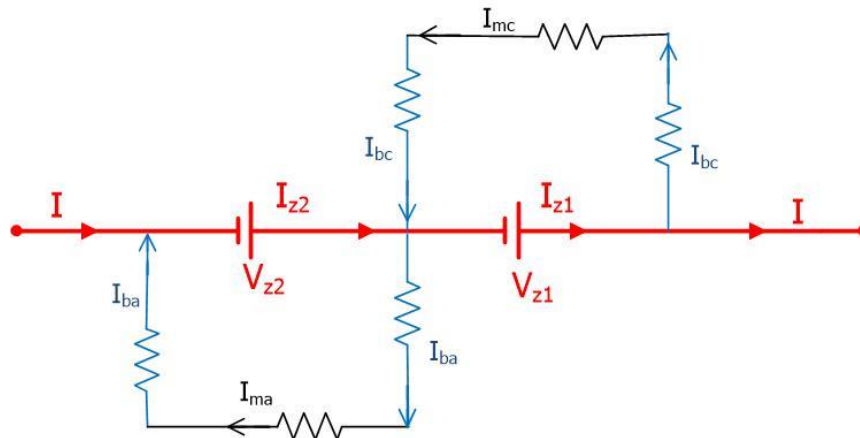
Figure 2.10 The shunt currents equivalent electric circuit of 2 cells in series

The resistance of main path and branch path are assumed to be equal. The current of each path can be calculated by:

$$I_{bc} = \frac{V_{z1}}{3 \cdot R_s}$$

$$I_{ba} = \frac{V_{z2}}{3 \cdot R_s}$$

$$I_{z1} = I + I_{bc}$$

$$I_{z2} = I_{ba} - I_{bc} + I_{z1}$$

The stack of 4-cells in series is showed below.
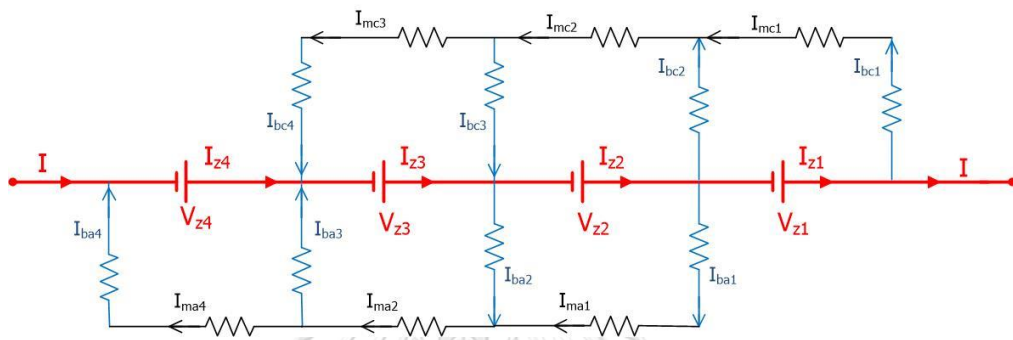
Figure 2.11 The shunt currents equivalent electric circuit of 4 cells in series

$$I_{bc2} = \frac{-5 \cdot V_{z1} + 6 \cdot V_{z2} + 2 \cdot V_{z3}}{21 \cdot R_s}$$

$$I_{bc3} = \frac{2 \cdot V_{z1} + 6 \cdot V_{z2} - 5 \cdot V_{z3}}{21 \cdot R_s}$$

$$I_{bc4} = \frac{V_{z1} + 3 \cdot V_{z2} + 8 \cdot V_{z3}}{21 \cdot R_s}$$

$$I_{mc2} = I_{bc4} + I_{bc3}$$

$$I_{bc1} = -I_{bc2} + I_{mc2}$$

$$I_{ba2} = \frac{-5 \cdot V_{z2} + 6 \cdot V_{z3} + 2 \cdot V_{z4}}{21 \cdot R_s}$$

$$I_{ba3} = \frac{2 \cdot V_{z2} + 6 \cdot V_{z3} - 5 \cdot V_{z4}}{21 \cdot R_s}$$

$$I_{ba4} = \frac{V_{z2} + 3 \cdot V_{z3} + 8 \cdot V_{z4}}{21 \cdot R_s}$$

$$I_{ma2} = I_{ba4} + I_{ba3}$$

$$I_{ba1} = -I_{ba2} + I_{ma2}$$

$$I_{z1} = I_{bc1} + I$$

$$I_{z2} = I_{z1} + I_{ba1} + I_{bc2}$$

$$I_{z3} = I_{z2} - I_{bc3} + I_{ba2}$$

$$I_{z4} = I_{z3} - I_{bc4} - I_{ba3}$$

The stack of 5-cells in series is showed below.
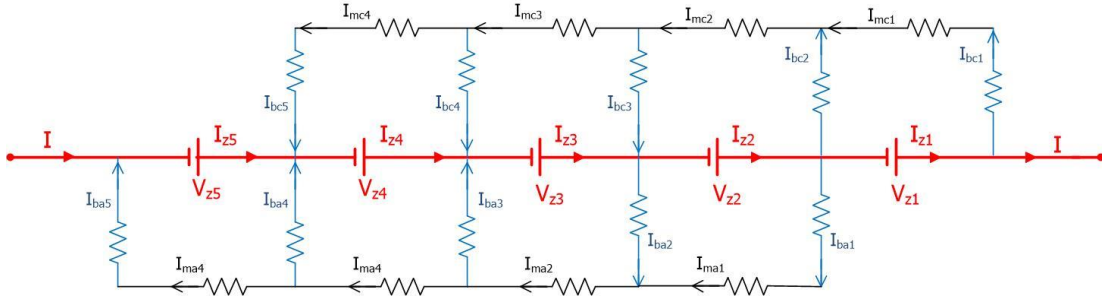
Figure 2.12 The shunt currents equivalent electric circuit of 5 cells in series

$$I_{bc2} = \frac{-13 \cdot V_{z1} + 16 \cdot V_{z2} + 6 \cdot V_{z3} + 2 \cdot V_{z4}}{55 \cdot R_s}$$

$$I_{bc3} = \frac{5 \cdot V_{z1} + 15 \cdot V_{z2} - 15 \cdot V_{z3} - 5 \cdot V_{z4}}{55 \cdot R_s}$$

$$I_{bc4} = \frac{2 \cdot V_{z1} + 6 \cdot V_{z2} + 16 \cdot V_{z3} - 13 \cdot V_{z4}}{55 \cdot R_s}$$

$$I_{bc5} = \frac{V_{z1} + 3 \cdot V_{z2} + 8 \cdot V_{z3} + 21 \cdot V_{z4}}{55 \cdot R_s}$$

$$I_{mc3} = I_{bc4} + I_{bc5}$$

$$I_{mc2} = I_{mc3} + I_{bc3}$$

$$I_{bc1} = -I_{bc2} + I_{mc2}$$

$$I_{ba2} = \frac{-13 \cdot V_{z2} + 16 \cdot V_{z3} + 6 \cdot V_{z4} + 2 \cdot V_{z5}}{55 \cdot R_s}$$

$$I_{ba3} = \frac{5 \cdot V_{z2} + 15 \cdot V_{z3} - 15 \cdot V_{z4} - 5 \cdot V_{z5}}{55 \cdot R_s}$$

$$I_{ba4} = \frac{2 \cdot V_{z2} + 6 \cdot V_{z3} + 16 \cdot V_{z4} - 13 \cdot V_{z5}}{55 \cdot R_s}$$

$$I_{ba5} = \frac{V_{z2} + 3 \cdot V_{z3} + 8 \cdot V_{z4} + 21 \cdot V_{z5}}{55 \cdot R_s}$$

$$I_{ma3} = I_{ba4} + I_{ba5}$$

$$I_{ma2} = I_{ma3} - I_{ba3}$$

$$I_{ba1} = -I_{ba2} + I_{ma2}$$

$$I_{z1} = I_{bc1} + I$$

$$I_{z2} = I_{z1} + I_{ba1} + I_{bc2}$$

$$I_{z3} = I_{z2} - I_{bc3} + I_{ba2}$$

$$I_{z4} = I_{z3} - I_{bc4} + I_{ba3}$$

$$I_{z5} = I_{z4} - I_{ba4} - I_{bc5}$$

2.4.3.10 Electrolyte system balance

The electrolyte system has been balanced the component in the electrolyte tank in order to calculate the battery with circulated electrolyte.

$$\frac{dC_{k,e}}{dt} = \frac{1}{V_{Et}}\left[F_{k,inE} - F_{k,outE} + 2 \cdot R_{D,e}\right] \qquad (2.75)$$

where $C_{k,e}$ is the concentration of species k in the electrolyte tank, V_{Et} is the volume of electrolyte solution in the tank, $F_{k,inE}$ is molar flow rate of species into the electrolyte tank which equal to the total molar flow rate out of the battery, $F_{k,outE}$ is molar flow rate of species out of the electrolyte tank which equal to the total molar flow rate flow into the battery.

2.4.3.11 Efficiency

The performance of the battery is evaluated by coulombic efficiency which is calculated by

$$Discharging\ coulombic\ efficiency = \frac{Q}{N_{zn,discharge} \cdot 2 \cdot F} \qquad (2.76)$$

$$Charging\ coulombic\ efficiency = \frac{N_{zn,deposited} \cdot 2 \cdot F}{Q} \qquad (2.77)$$

จุฬาลงกรณ์มหาวิทยาลัย

CHULALONGKORN UNIVERSITY

Chapter 3

Methodology

3.1 Modelling and validation of zinc-air battery

The model is developed under assumptions including

- The batteries are the isothermal system at 298 K.
- No concentration gradient in the same region.
- Convective transfer between the electrodes is neglected.
- Electrochemical reactions occur on the electrode surface
- Zinc-metal occurs on the surface of the electrode. It does not flow out of the battery.
- No influence of the deposited zinc-metal on the flow
- The electrolyte volume is constant.

Then, the model was simulated by MATLAB software. The voltage and current density were evaluated in single-cell and the connected cells. The I-V curve consisted of consecutive charge or discharge step varying current with holding time of 120 s. The voltage of full-cell and half -cell were measure. Half-cell voltages were compared to reference electrodes that are zinc plate and Hg/HgO. The cell potential at the end of holding time was taken to plot the polarization curves.

3.1.1 The experiment of single-cell

The validation method is conducted by the experiment of single-cell of zinc-air flow battery which showed in figure 3.1.
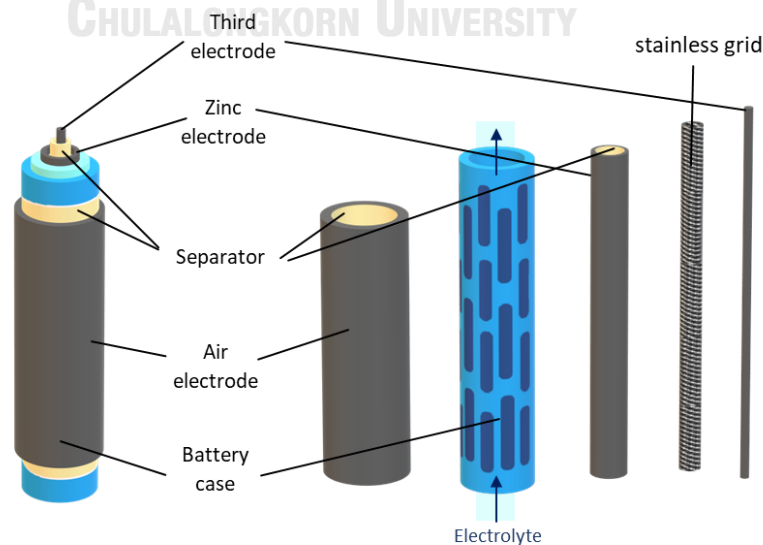
Figure 3.1 The component of tube zinc-air flow battery

Figure 3.2 The real component of tube zinc-air flow battery

The experiment was conducted by a cylindrical zinc-air flow battery. The electrodes fabricate with the cellular PVC tube (figure 3.2). Air electrode (figure 3.3b) which consisted of 3 layers. First, the outer layer was gas diffusion layer. It comprised of PTFE 40%, carbon 40% for conductivity and some of glucose. The middle layer was Ni foam which was current collector. Another layer comprised of carbon 70% and manganese oxide 30%. The air electrode attached to separator and then attached to the battery case. The separator (figure 3.3a) was made by coating PVAc on the filter paper. Inside of PVC tube was fulfilled with the electrolyte and it consisted of zinc electrode, another separator attached on the stainless grid and the innermost was the third electrode. The zinc electrode and third electrode were made by Ni foam. The electrolyte flowed from below to upper and flowed to the electrolyte tank then circulating into the bottom of the battery again.
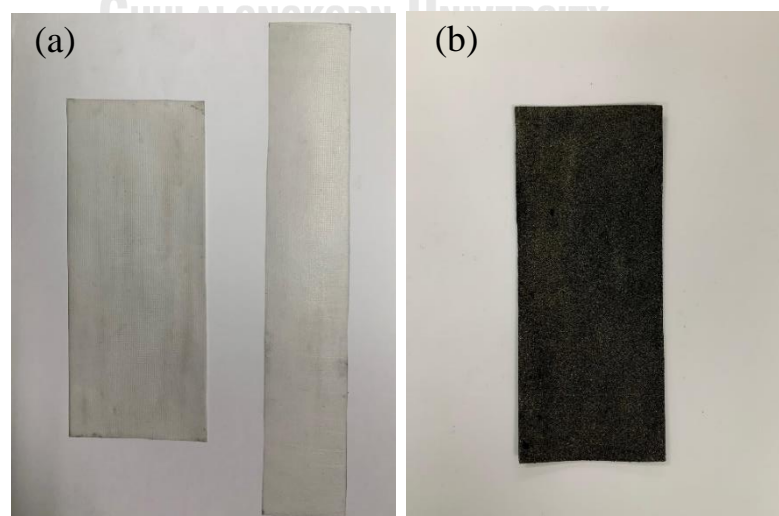
Figure 3.3 The real component of tube zinc-air flow battery (a) separator, (b) Air electrode

3.1.2 The experiment of 3-cells in series

Three-cells of the battery were connected in series as shown in figure 2.7. The equivalent circuit was showed in figure 2.9. In the experiment (figure 3.4), when setting up to collecting data, amp meters were used between the cells to measure the passing current. So, the experiment of 3-cells in series was conducted follow figure 3.5.

Figure 3.4 The experiment of 3-cells with flowing electrolyte
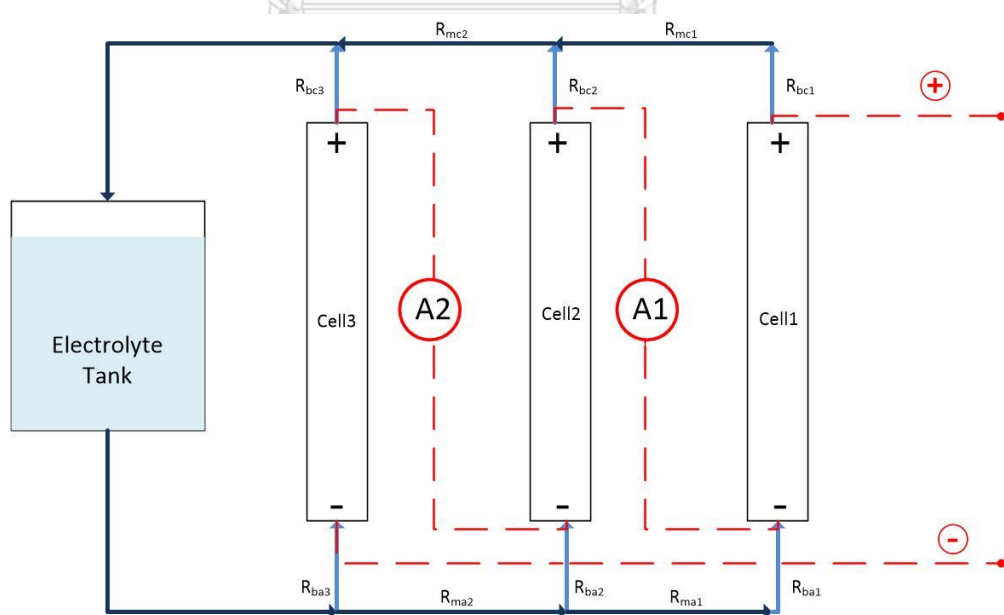
Figure 3.5 Battery flow paths between 3-cells battery connected in series with amp meters

3.1.3 The experiment of 3-cells in parallel

Three-cells of batteries connected in parallel and each current path had amp meter to measure the current showed in figure 3.6.
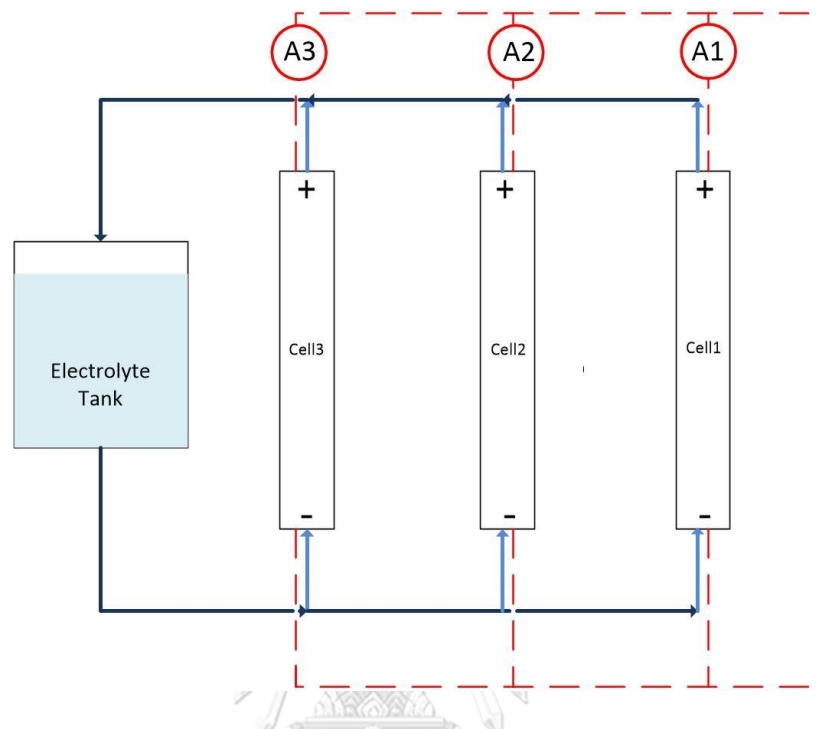
Figure 3.6 Battery flow paths between 3-cells battery connected in parallel with amp meters

3.2 Studied parameters in the model

After modeling, the battery simulation will be varied by the studied parameter: number of cells connected, current density, electrolyte flow rate and electrolyte flow path resistance as mention in table 1.4. In parts of electrolyte concentration, the value is fixed at 8 M KOH with 0.5 M ZnO. Then, the effect of these parameters on the current loss due to shunt current will be evaluated.

3.3 Validation and analysis method

The simulation result will be compared to the experimental data. Some parameters have to adjust to fit with the experiment. The model that validated with experiment will be used to develop the stack series of battery in order to investigate the effect of studied parameter.

Table 3.1 List of symbols

Symbol	Description	Unit
a_0	initial solid-solution interface	dm^2/dm^3
A_{air}	active area of air electrode	dm^2
a_c	effective areas	dm^2/dm^3
A_{cell}	area of the cell	dm^2
A_{elec}	area of electrolyte	dm^2
a_s	solid-solution interface	dm^2/dm^3
A_{sep}	area of separator	dm^2
A_{zn}	area of zinc electrode	dm^2
C_{dl}^{air}	double layer capacitance of the air electrode	F/dm^2
C_{dl}^{zn}	double layer capacitance of the zinc electrode	F/dm^2
$C_{k,b}$	Concentration of species k in bulk	mol/dm^3
$C_{k,s}$	Concentration of species k in zinc electrode surface	mol/dm^3
$C_{k,a}$	Concentration of species k in air electrode	mol/dm^3
d_{in}	inner diameter of electrolyte channel	dm
d_{eq}	hydraulic diameter	dm
D_k	diffusivity of species k in the electrolyte	dm^2/s
d_{out}	outer diameter of electrolyte channel	dm
E_0^{air}	standard potential of air electrode	V
E_0^H	standard potential of HER	V
E_0^{zn}	standard potential of zinc electrode	V
F	Faraday constant	C/mol
$F_{k,in}$	molar flow rate of species k into bulk	mol/s
$F_{k,out}$	molar flow rate of species k out of bulk	mol/s
i_0^{ref}	reference exchange current density	A/dm^2
i_r	current density produced or consumed by reaction r	A/dm^2
J_k	molar transfer rate of species k across electrode	mol/s

J_k^{dif}	diffusion transfer of species k	mol/s
$J_k^{dif,s}$	diffusion transfer of species k across zinc electrode surface and bulk	mol/s
J_k^{mig}	migration transfer of species k	mol/s
k_s	rate constant of zinc precipitation	dm³/s
l	length of the electrode	dm
n	number of exchange electron in reaction	-
N_k	mol of species k	mol
R	gas constant	J/mol•K
R_b	resistance of branch shunt path	Ω
R_{com}	resistance of battery component	Ω•dm
R_m	resistance of main shunt path	Ω
R_{ohm}	ohm resistance	Ω
R_s	resistance of shunt path	Ω
R_k^r	reaction rate of species k in reaction r	mol/s
Re	Reynold number	-
Sc	Schmidt number	-
Sh	Sherwood number	-
T	temperature	K
v	electrolyte volumetric flow rate	dm³/s
V_{solid}	volume of solid on the zinc electrode	dm³
$\bar{V}_k$	specific volume of species k	dm³/mol
V_e^{air}	volume electrolyte in air electrode	dm³
V_e^{zn}	volume electrolyte in zinc electrode	dm³
X_{zn}	active surface fraction of zinc	-
z_k	ion number of species k	-
α	transfer coefficient of the reaction	-
δ_{active}	reaction zone thickness of air electrode	dm
δ_{com}	component thickness	dm

$\delta_{k,dif}$	diffusion layer thickness	dm
δ_{GDL}	GDL thickness	dm
δ_{sep}	separator thickness	dm
δ_{zn}	zinc electrode thickness	dm
ε	porosity of zinc electrode	-
ε_0	initial porosity of zinc electrode	-
ε_{sep}	porosity of separator	-
η_{act}^{r}	activation loss of reaction r	V
η_{ohm}	ohmic loss	V
μ	viscosity of electrolyte	Pa/s
ρ	density of electrolyte	g/dm^3
σ	conductivity	S/dm
υ_k^r	stoichiometric coefficient of species k in reaction r	-

Table 3.2 Designed parameters of battery

Parameter	Value	Source of the value
$a_0\ for\ charge$	1	Validated
$a_0\ for\ discharge$	0.01	Validated
A_{air}	0.52	Validated
a_c	1×10^5	(Mao 1992)
A_{rd}	0.15	Validated
$C_{O_2,ref}$	1.9446×10^{-5}	(Tromans 1998)
$C_{Zn(OH)_4{}^{2-},sat}$	$-0.21 + 0.0975C_{KOH}$ $+ 0.00125C_{KOH}^2$	(Stamm, Varzi et al. 2017)
C_{dl}^{air}	1.4	(Schröder 2016)
C_{dl}^{zn}	0.02	(Schröder 2016)
$D_{H_2O\ in\ KOH}$	5.26×10^{-7}	(Schröder and Krewer 2014)
$D_{K^+\ in\ KOH}$	1.2×10^{-7}	(Schröder and Krewer 2014)

$D_{O_2 \ in \ air}$	2.3×10^{-3}	(Schröder 2016)
$D_{O_2 \ in \ KOH}$	$(0.47026 + 1.3619 \cdot \exp(\frac{-C_{OH^-}}{3.15255})) \cdot 10^{-7}$	(Schröder 2016)
$D_{OH^- \ in \ KOH}$	$\dfrac{1.3806 \times 10^{-23} \cdot T}{6 \cdot \pi \cdot \mu \cdot 4.642 \times 10^{-11}} \times 10^2$	(Schröder 2016)
$D_{Zn(OH)_4^{2-} \ in \ KOH}$	6×10^{-8}	(Dundálek, Šnajdr et al. 2017)
$i_0^{air,ref}$	$1.5\times10{-8}$	(Mao 1992)
$i_0^{zn,ref}$	$0.0281 + 0.0613 C_{OH^-} - 0.0041 C_{OH^-}{}^2$	(Lao-atiman, Bumroongsil et al. 2019)
k_s	0.25	(Schröder and Krewer 2014)
$R_{com} \ for \ charge$	0.12	Validated
$R_{com} \ for \ discharge$	1.05	Validated
$\bar{V}_{H_2O}$	1.78×10^{-2}	(Schröder 2016)
$\bar{V}_{OH^-}$	7.89×10^{-3}	(Schröder 2016)
$\bar{V}_{Zn}$	9.15×10^{-3}	(Schröder and Krewer 2014)
$\bar{V}_{ZnO}$	1.45×10^{-2}	(Schröder and Krewer 2014)
$\bar{V}_{Zn(OH)_4^{2-}}$	1.86×10^{-2}	(Schröder and Krewer 2014)
α	0.5	Assumed
δ_{active}	0.015	Validated
$\delta_{filmair}$	0.005	Validated
μ	$0.799533504 \cdot \exp(0.155921614 C_{OH^-}) \cdot 10^{-3}$	(Schröder 2016)
ρ	$-0.4931 C_{OH^-}{}^2 + 45.761 C_{OH^-} + 999.63$	(Gilliam, Graydon et al. 2007)
σ_{elec}	$(-0.00342T + 1.197 \times 10^{-5} \cdot T^2 - 1.173 C_{KOH} - 0.00517 C_{KOH}^2 + 0.00328T \cdot C_{KOH} + 119.6 \cdot \frac{C_{KOH}}{T} + 0.000624 C_{KOH}^3 - 1.883 \times 10^{-7} \cdot T^2 \cdot C_{KOH}^2) \cdot 10$	(See and White 1997)
σ_{Zn}	2×10^6	(Sunu and Bennion 1980)
σ_{ZnO}	1×10^{-9}	(Schröder and Krewer 2014)

Table 3.3 Initial condition

Parameter	Value
C_{H_2O}	48.51
C_{K^+}	8
C_{O_2}	0.00847
C_{OH^-}	7.2
$C_{Zn(OH)_4{}^{2-}}$	0.5
$N_{Zn}\ for\ charge$	0
$N_{Zn}\ for\ discharge$	0.1538
N_{ZnO}	0
ε_0	0.8
η_{act}	0

The methodology of this research is showed as the flow chart as following.
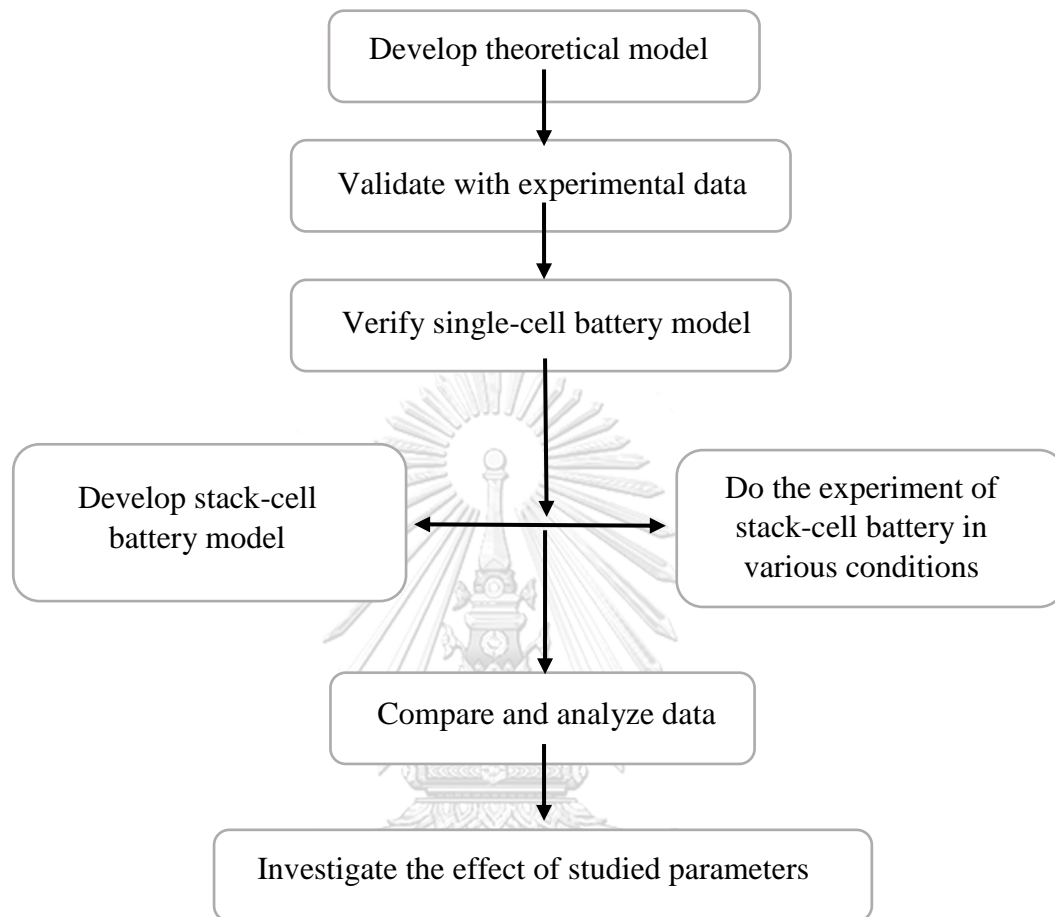
Figure 3.7 The methodology flow chart of the research

Chapter 4

Result and Discussion

4.1 Validation

For this section, the polarization curve was plotted by collecting the voltage at each current. The results from the simulation were validated with the experimental data. Some of the parameters were adjusted until the polarization curves from simulation and experimentation were fitted.

$$E_{cell} = E^{air} - E^{zn} - \eta_{act}^{zn} - \eta_{act}^{air} - \eta_{ohm} \qquad (2.60)$$

The collecting data consisted of full cell voltage and half-cell voltage with the two reference electrodes that are zinc plate and Hg/HgO. As mention in equation 2.60, each obtained voltage from experimental data represents the difference of potential from simulation data as described in the table below. These voltages will be used in the graph and the following content.

Table 4.1 The potential representation and the calculation

Voltage	Simulation data	Experimental data
E_{cell}	$E^{air} - E^{zn} - \eta_{act}^{air} - \eta_{act}^{zn} - \eta_{ohm}$	V_{zn} VS V_{air}
V_{zn} VS NHE	$E^{zn} + \eta_{act}^{zn} + x \cdot \eta_{ohm}$	V_{zn} VS Hg/HgO $+ 0.098$
V_{air} VS NHE	$E^{air} - \eta_{act}^{air} - (1 - x) \cdot \eta_{ohm}$	V_{air} VS Hg/HgO $+ 0.098$
V_{zn} VS Zn/Zn^{2+}	$\eta_{act}^{zn} + x \cdot \eta_{ohm}$	V_{zn} VS Zn/Zn^{2+}
V_{air} VS Zn/Zn^{2+}	$E^{air} - E^{zn} - \eta_{act}^{air} - (1 - x) \cdot \eta_{ohm}$	V_{air} VS Zn/Zn^{2+}

4.1.1 Discharging process

According to tables 3.2 and 4.1, the parameters: $A_{air}, \delta_{active}, R_{comp}, x$ and a_0 must be validated. It cannot measure. The active area of the air electrode (A_{air}) is possible to lower than the measurement. The loss area resulting from attached area, lacking catalyst area or non-wetting area. The thickness of active zone (δ_{active}) is where the oxygen reduction reaction (ORR) takes place. The cell component resistance (R_{comp}) is the resistance of battery. It causes ohmic loss that increases with current. Ohmic loss (η_{ohm}) is divided into two parts when measuring half-cell voltage data. x-factor in table 4.1 is the proportion of η_{comp} that occurs at the zinc electrode. Lastly, the solid-solution interface area per unit volume (a_0) also cannot measure.

The polarization results from the experiment show that varying flow rate doesn't affect much on voltage same as to the simulation results. These results show

in the appendix. Thus, the polarization curve is fitted by one condition that is KOH 8M, initial zincate 0.5M and flow rate 0.75 cm/s or Reynold number 12.5.

The overpotential at the low current density occurs from activation loss. Then, when increasing the current density, the activation loss is constant. So, the overpotential in later increases from ohmic loss. And, the ohmic loss increase with current density. The simulation curve will be fitted with experimental data by adjusting the parameter. A_{air} can shift the curve in x-axis direction. Increasing δ_{active} can increase i_0^{air} in equation 2.45 leading to the activation loss of air electrode decreasing. Thus, adjusting δ_{active} can shift the air electrode curve in y-axis direction. In the same way, adjusting the a_0 can shift the zinc electrode curve in y-axis direction. Increasing R_{comp}, the slope of the curve is increased as mention above.

Figure 4.1 The comparison of half-cell voltage of zinc electrode in the discharging battery between experimental data (dot) and simulation (line): (a.) using zinc plate as reference electrode and (b.) comparing with NHE
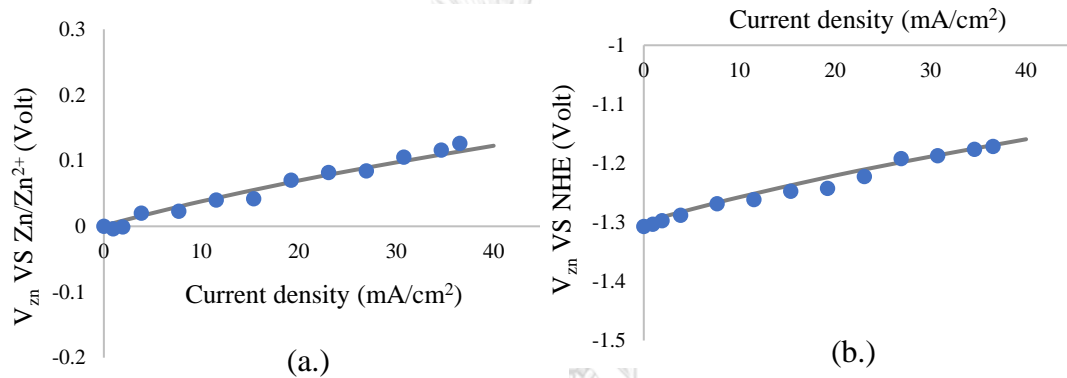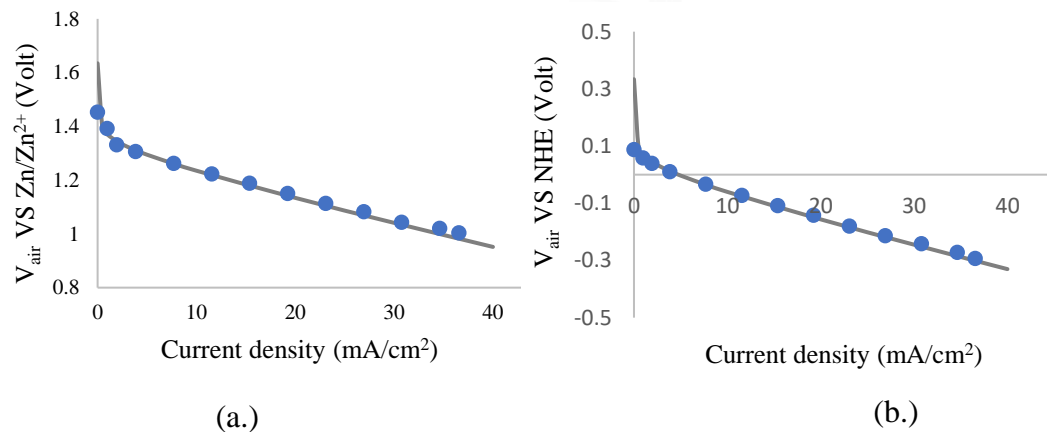

Figure 4.2 The comparison of half-cell voltage of air electrode in the discharging battery between experimental data (dot) and simulation (line): (a.) using zinc plate as reference electrode and (b.) comparing with NHE

Figures 4.1 and 4.2 show that the half-cell voltage can be fitted with experimental data. In figure 4.1a, zinc electrode voltage compared to zinc plate expresses the overpotential at zinc electrode which is activation loss and some portion of ohmic loss. So, the activation loss of zinc electrode (η_{act}^{zn}) in the model is validated by this curve. This method also conducted by Deiss, Holzer et al. (2002). The zinc electrode voltage compared to NHE in figure 4.1b expresses total voltage of zinc electrode. It includes the potential of zinc electrode (E^{zn}). For this reason, the half-cell voltage of zinc electrode in the model has more accurate when using two reference electrodes.

Also, the half-cell voltage of air electrode is fitted same as to the half-cell of zinc electrode. In figure 4.2a, air electrode voltage compared to zinc plate shows the potential of full cell minus the activation loss and ohmic loss of zinc electrode. And, the air electrode voltage compared to NHE in figure 4.2b shows the potential of air electrode and another portion of ohmic loss. Although the half-cell voltage of air electrode in the experiment is compared to two reference electrodes, the potential (E^{air}) and activation loss (η_{act}^{air}) of air electrode cannot be separated to validate.
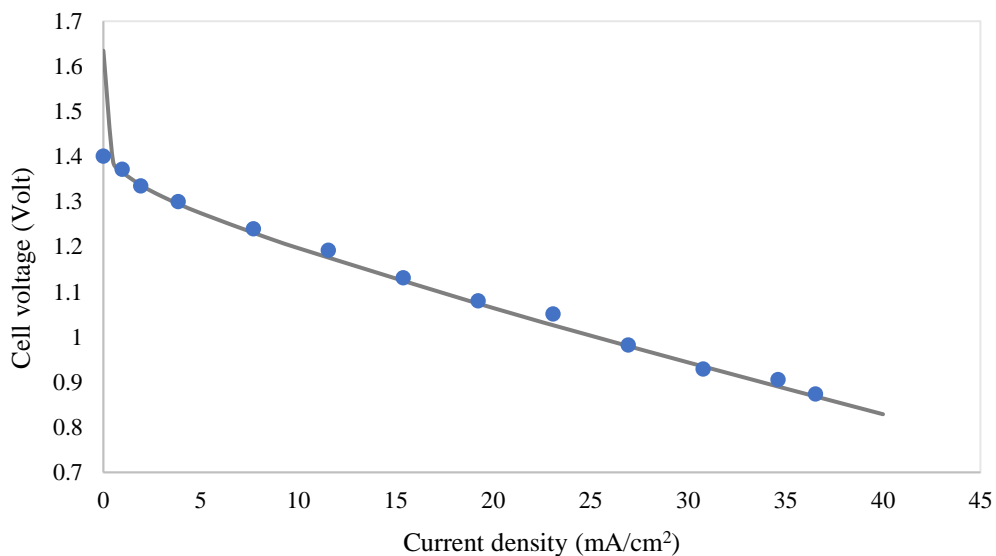

Figure 4.3 The comparison of cell voltage of the discharging battery between experimental data (dot) and simulation (line)

The validation of the polarization curve shows in figure 4.3. The simulation fit with the experimental data. The adjusted parameters: A_{air} is 52 cm^2, δ_{active} is 1.5 mm, R_{comp} is 1.05 $\Omega \cdot dm$, x is 0.15 and a_0 is 0.01 dm^2/dm^3.

These adjusted parameters show that air electrode area is lower than actual size. It could result from the area that used to attach the electrode to the battery and the catalyst loss. The thickness of active zone is calculated by thickness of gas diffusion layer (1.3 mm), catalyst layer and interface layer of electrode and electrolyte which the reaction taking place. x means that 15% of ohmic loss occurred at zinc electrode and 85% of ohmic loss occurred at air electrode. It could result from the

area of zinc electrode is lower than the area of air electrode. Lastly, a_0 is very low because the initial value of zinc metal in zinc electrode quite dense in the Ni foam in discharging process.

4.1.2 Charging process

Same as discharging process, the parameters: $A_{rd}, \delta_{filmair}, R_{comp}, x$ and a_0 must be validated. The active area of the third electrode (A_{rd}) is possible to lower than the measurement. The loss area resulting from attached area and bubble that obstructs the surface. The thickness of active zone ($\delta_{filmair}$) is where the oxygen evolution reaction (OER) takes place. The cell component resistance (R_{comp}) which causes ohmic loss. Ohmic loss (η_{ohm}) is also divided into two parts when measuring half-cell voltage data. x portion for zinc electrode and 1-x portion for the third electrode as mention before.

The results from experimentation show that varying flow rate doesn't affect much on voltage same as to the simulation results. The result showed in appendix. Thus, the polarization curve is fitted by one condition that is KOH 8M, initial zincate 0.5M and flow rate 0.75 cm/s or Reynold number 12.51.

Like discharging process, the simulation curve will be fitted with experimental data by adjusting the parameter. A_{rd} can shift the curve in x-axis direction. Adjusting $\delta_{film\ air}$ can shift the air electrode curve in y-axis direction same as to δ_{active}. In the same way, adjusting the a_0 can shift the zinc electrode curve in y-axis direction. Increasing R_{comp}, the slope of the curve is increased as mention above.

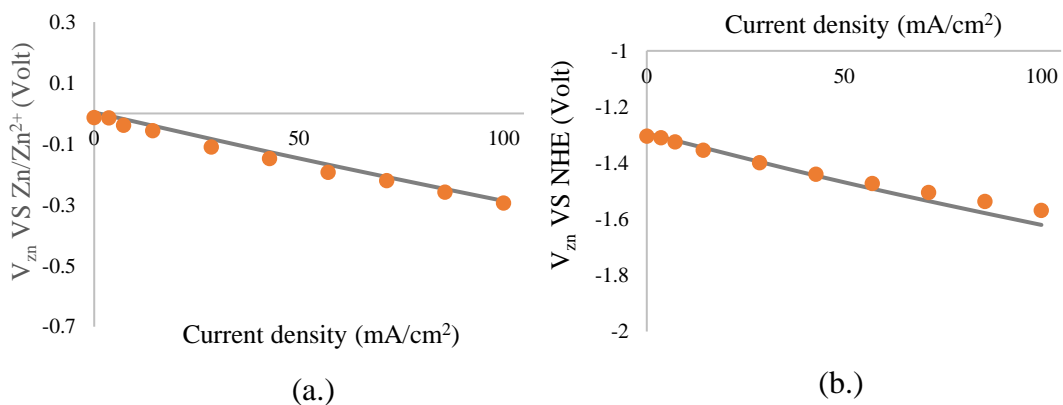

(a.)   (b.)

Figure 4.4 The comparison of half-cell voltage of zinc electrode in the charging battery between experimental data (dot) and simulation (line): (a.) using zinc plate as reference electrode and (b.) comparing with NHE
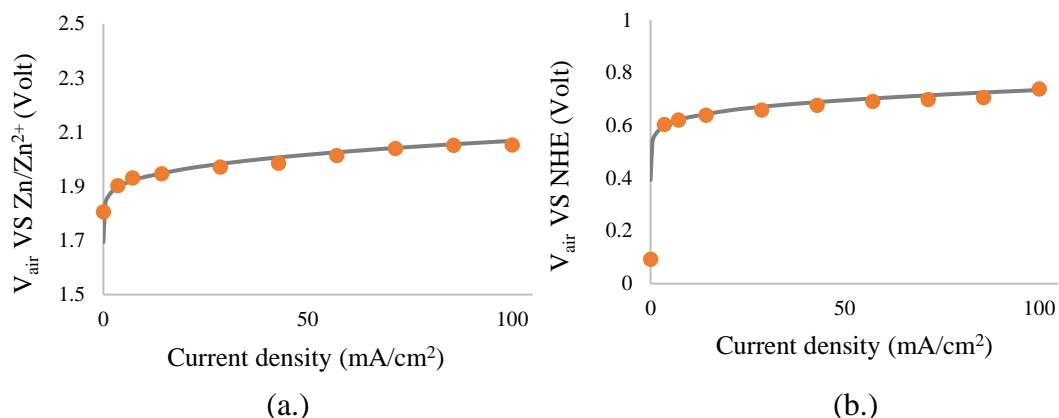
(a.)   (b.)

Figure 4.5 The comparison of half-cell voltage of third electrode in the charging battery between experimental data (dot) and simulation (line): (a.) using zinc plate as reference electrode and (b.) comparing with NHE

Figures 4.4 and 4.5 show that the half-cell voltage can be fitted with experimental data. The meaning of voltage in each curve is same as discharging process described before. Compare to discharge (figure 4.1 and 4.2), the polarization curve is in opposite side. In discharging process, overpotentials have positive value. When increasing current density, zinc potential has less negative and air potential is lower. The cell potential also drops. According to high current density, battery loss more potential to passage the current through the resistance. In contrast, charging process (figure 4.4 and 4.5), overpotentials have negative value. When increasing current density, zinc potential has more negative and air potential is high. The gap between two electrodes increases. The cell potential also increases. Thus, high current density, battery use more potential to passage the current through the resistance.
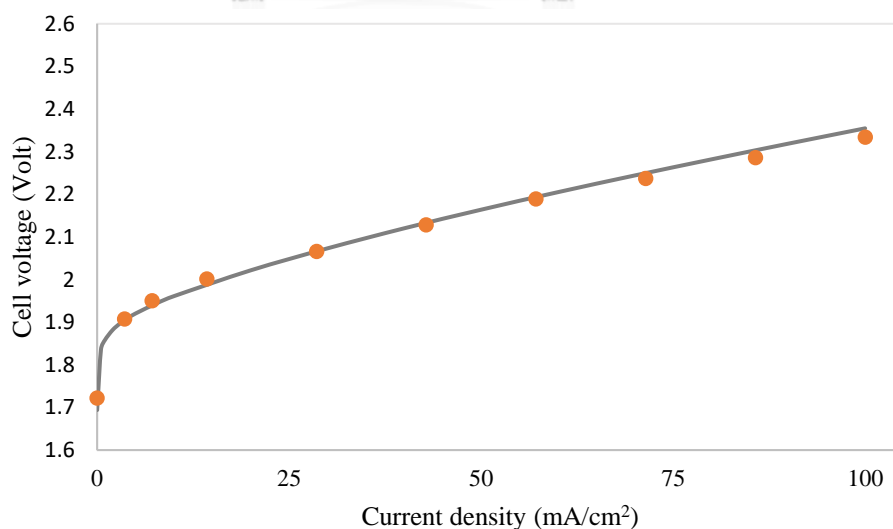

Figure 4.6 The comparison of cell voltage of the discharging battery between experimental data (dot) and simulation (line)

The validation of the polarization curve shows in figure 4.6. The simulation fit with the experimental data. The adjusted parameters: A_{rd} is 15 cm^2, $\delta_{film\ air}$ is 0.5 mm, R_{comp} is 0.12 $\Omega \cdot dm$, x is 0.9 and a_0 is 1 dm^2/dm^3.

These adjusted parameters show that the third electrode area is lower than actual size. It could result from the space that used to attach the electrode to the battery and the obstructive bubble. The thickness of active zone is the thickness which the reaction taking place. $\delta_{film\ air}$ is lower than the thickness of the third electrode. It means that OER takes place in the electrode. x means that 90% of ohmic loss occurred at zinc electrode and 10% of ohmic loss occurred at third electrode. It could result from the area of zinc electrode is higher than the area of third electrode. Lastly, a_0 is more than discharging process because the initial value of zinc metal in zinc electrode has very small in the Ni foam in charging process

4.2 Connected cells in series

4.2.1 Current path

The connected pattern of 3-cells in series showed in figure 2.7. The current leaks through the electrolyte flow path. It is shunt current. The experiment is done to compare the result with the simulation. The resistance of electrolyte flow path is validated. In experiment, amp meter is used to measure between the cell as shown in figure 4.7. So, the current paths which can validate are I_{A1} and I_{A2}.
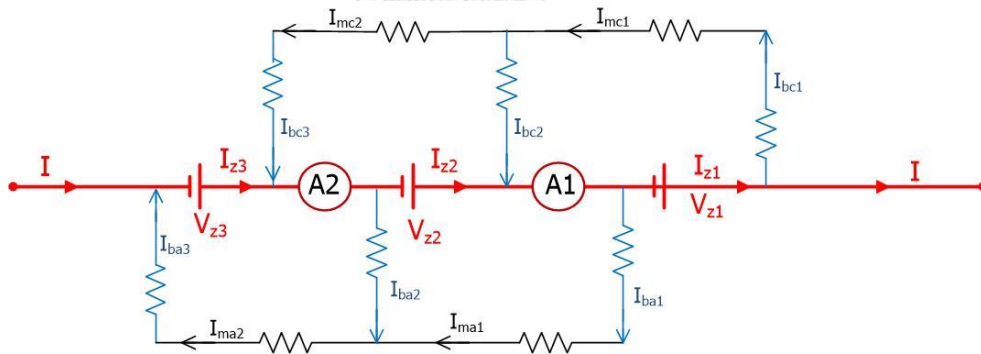
Figure 4.7 The equivalent electric circuit with current direction and amp meters

Therefore, the collecting current by amp meters is not only current passing battery, but it includes some leakage currents showed in equation below.

$$I_{A1} = I_{z2} + I_{bc2} \tag{4.1}$$
$$I_{A2} = I_{z3} + I_{bc3} \tag{4.2}$$
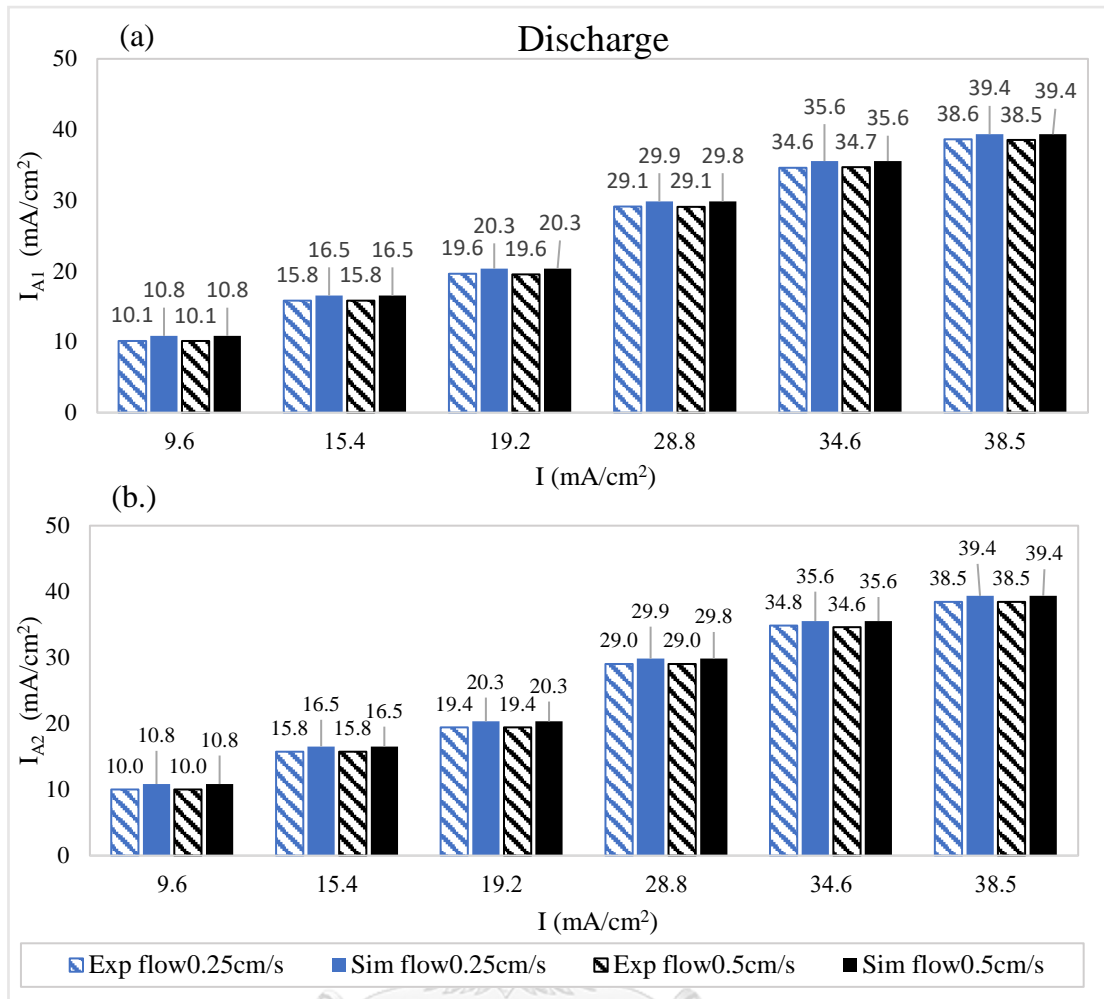
Figure 4.8 The comparison of currents (a) I_{A1} and (b) I_{A2} with the discharging currents between experimental data (line) and simulation (thick) in low flow rate (blue) and high flow rate (black)

All experimental data is in appendix. The current I_{A1} and I_{A2} of experiment and simulation are compared in figure 4.8 and 4.9.

$$R_m = \frac{L_m}{\sigma_{elec} \cdot A_{elecTube}} \tag{2.73}$$

$$R_b = \frac{L_b}{\sigma_{elec} \cdot A_{elecTube}} \tag{2.74}$$
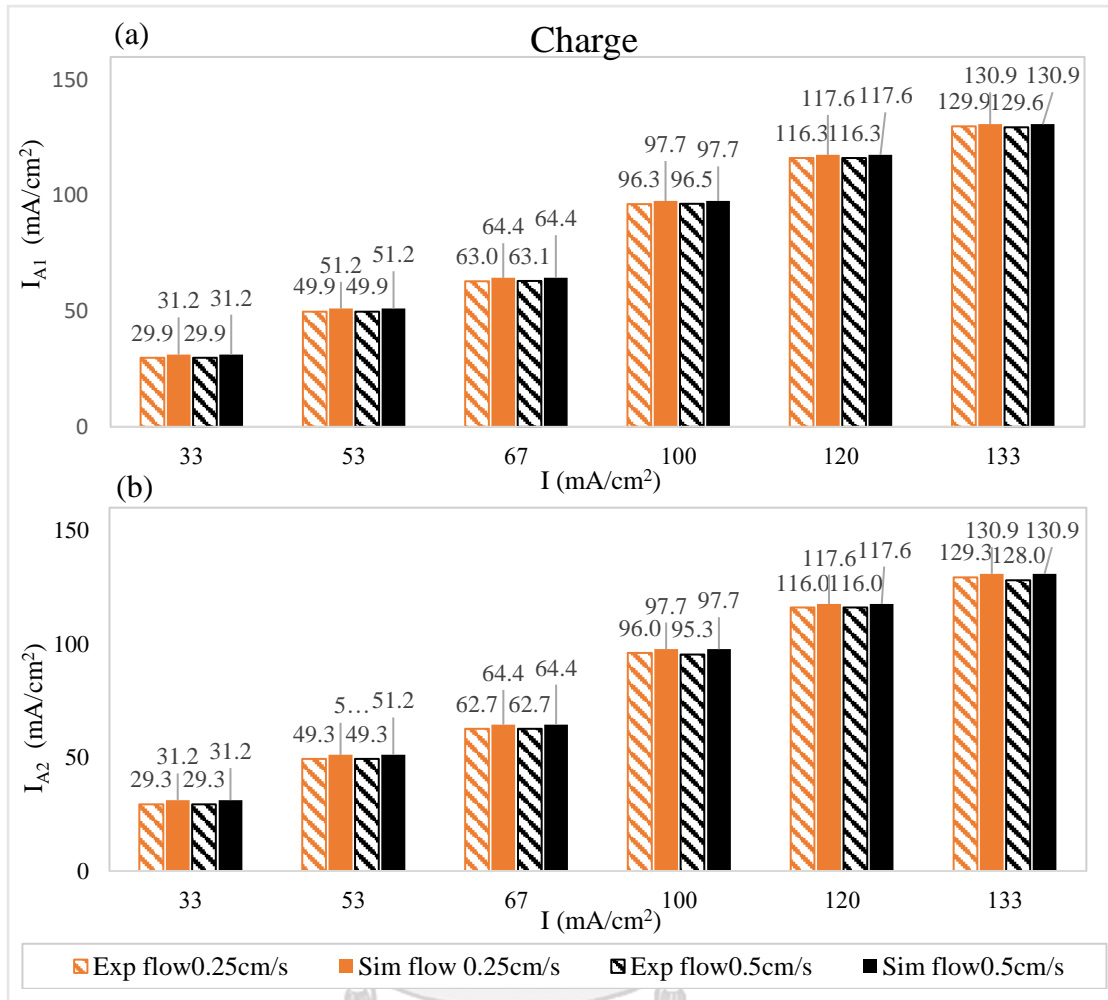
Figure 4.9 The curve of currents (a) I_{A1} and (b) I_{A2} with the charging currents comparing between experimental data (line) and simulation (thick) in low flow rate (orange) and high flow rate (black)

The resistance of electrolyte flow path calculated by equation 2.73 and 2.74. L_b and L_m are 8 cm. And, $A_{elecTube}$ is 1.33 cm^2. So, R_m and R_b is 9.8 Ω The results show that the current from simulation almost equal to the experiment. The simulation results are a bit higher because the manifold is not smooth. Some resistance cannot totally measure such as the joint which affects to the $A_{elecTube}$ like Jupudi, Zappi et al. (2007) research. They considered the inlet and outlet port of electrolyte in a bipolar electrolyzer stack and the effect of each resistance component were studied. In this work, the joints or inlet/outlet port are neglected.

From figure 4.8 and 4.9, the value of I_{A1} and I_{A2} in different flow rates is nearly the same because of small gap of flow rate. For this reason, flow = 0.25 cm/s is chosen to compare Voltage.

4.2.2 Leakage current
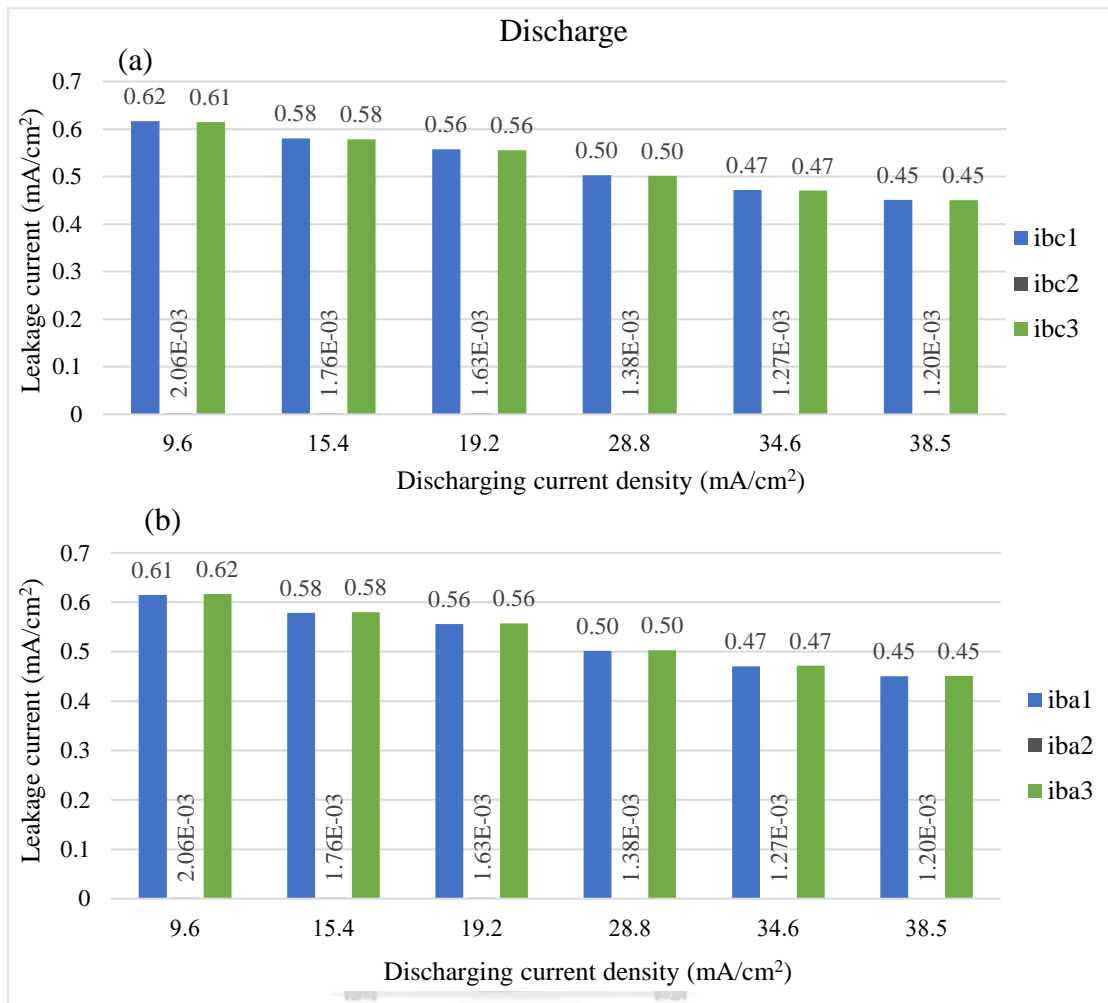
Figure 4.10 The leakage currents (a) Ibc and (b) Iba in each electrolyte path of 3-cells connected in series as a function of discharging currents

CHULALONGKORN UNIVERSITY

By comparing experiment data and simulation data, the result of current is nearly the same. This model has high accuracy. Leakage current can find from simulation in both discharging and charging process as shown in figure 4.10 and 4.11

From figure 4.10, increasing of discharging current has lower leakage current. The leakage current at top and bottom of the battery is the same and symmetrically. The direction of current shown in figure 4.7. The middle electrolyte line has the lowest leakage current. All current calculated by Kirchoff's Laws as shown in section 2.4.3.9
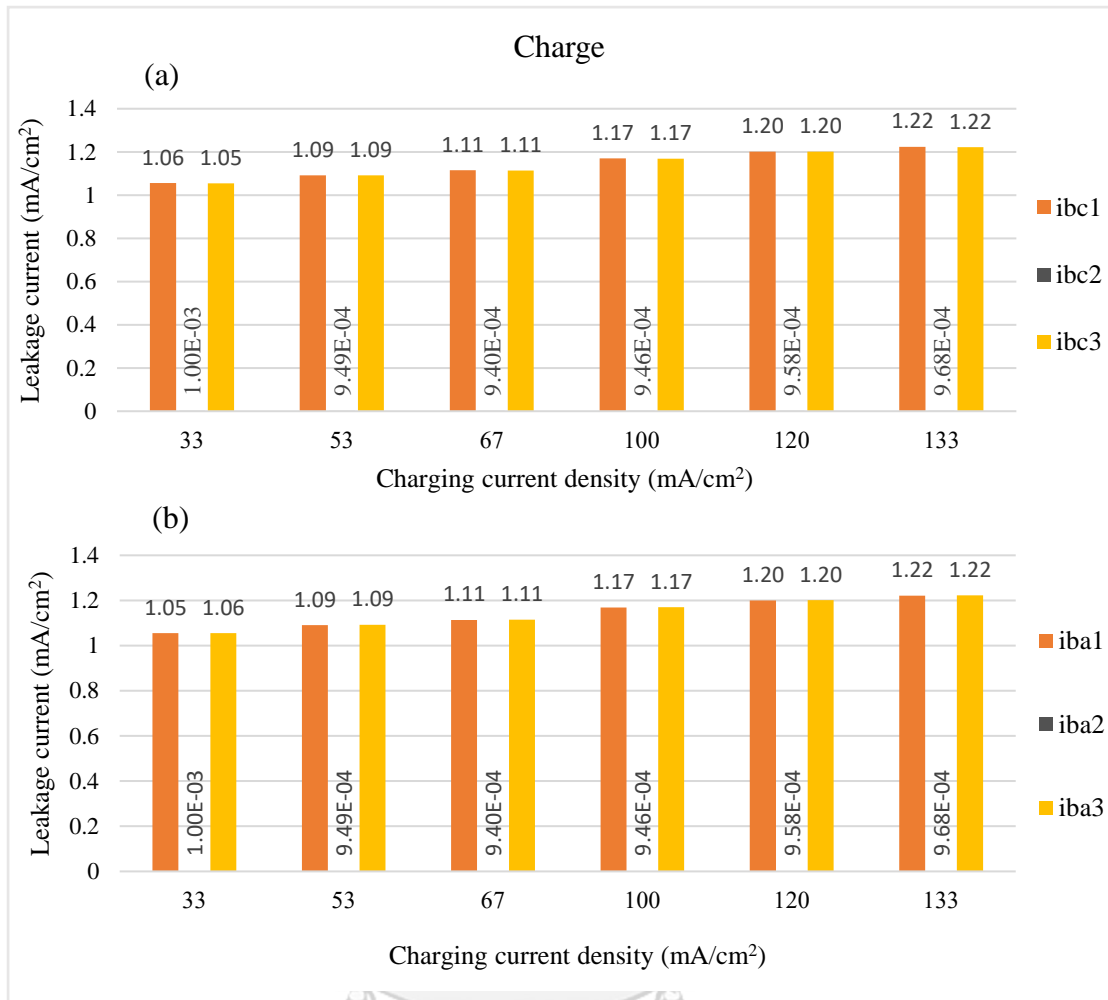
Figure 4.11 The leakage currents (a) Ibc and (b) Iba in each electrolyte path of 3-cells connected in series as a function of charging currents

On the other hand, the main current during charge (red line from figure 4.7) has opposite direction compare with during discharging. But the direction of leakage current (blue line from figure 4.7) has same direction. Leakage current during charging shown in figure 4.11. When increasing charging current, leakage current also increases.

4.2.3 Cell voltage

In the experiment, total of voltage and voltage of each cell were collected. This data is compared in the figure below.
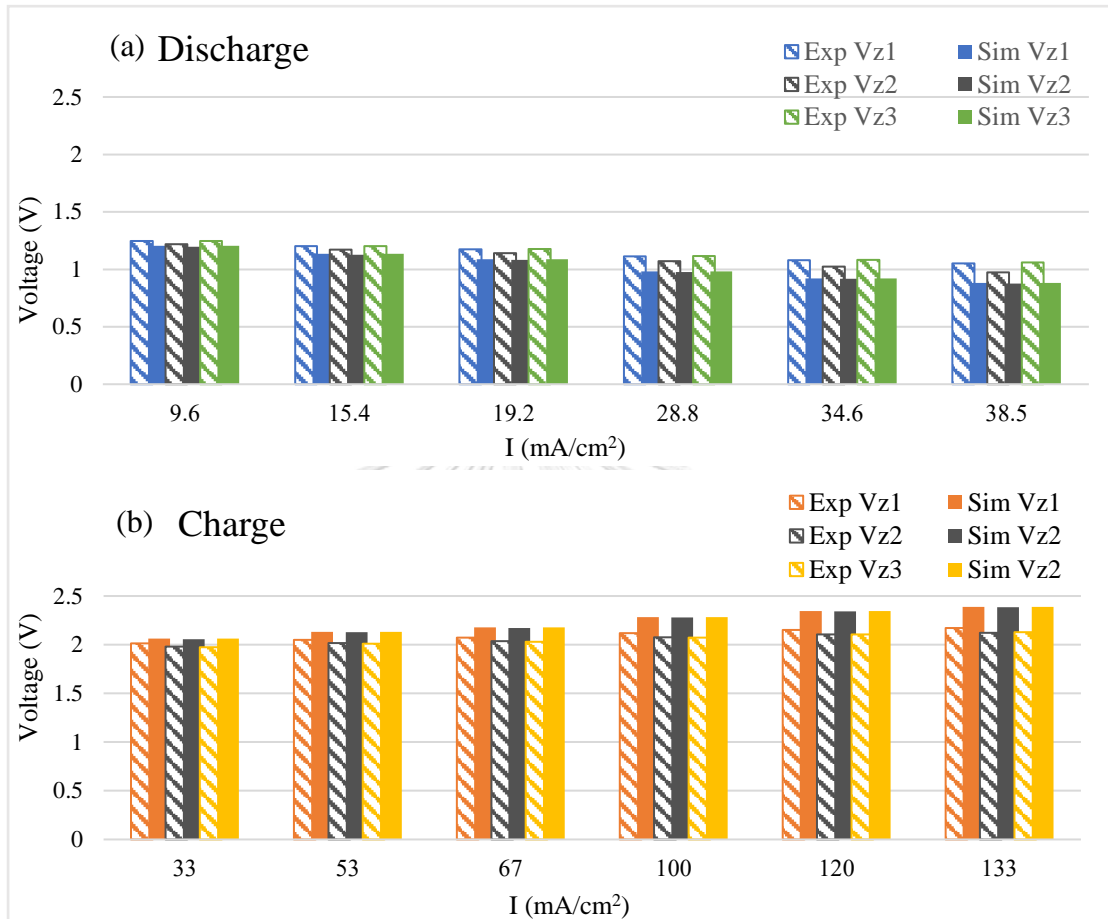
Figure 4.12 The comparison of (a) discharge and (b) charge voltage of each cell between experimental data (line) and simulation (thick)

From figure 4.12, at low current density value, the voltage from the simulation is equal to the voltage from the experiment. On the other hand, the difference in voltage seems to be higher in higher current density. During discharging, the voltage of experiment is higher than simulation. And, during charging, voltage of experiment is lower than simulation. Due to ohmic loss of this battery is lower than the validated model.

4.2.4 Voltage loss
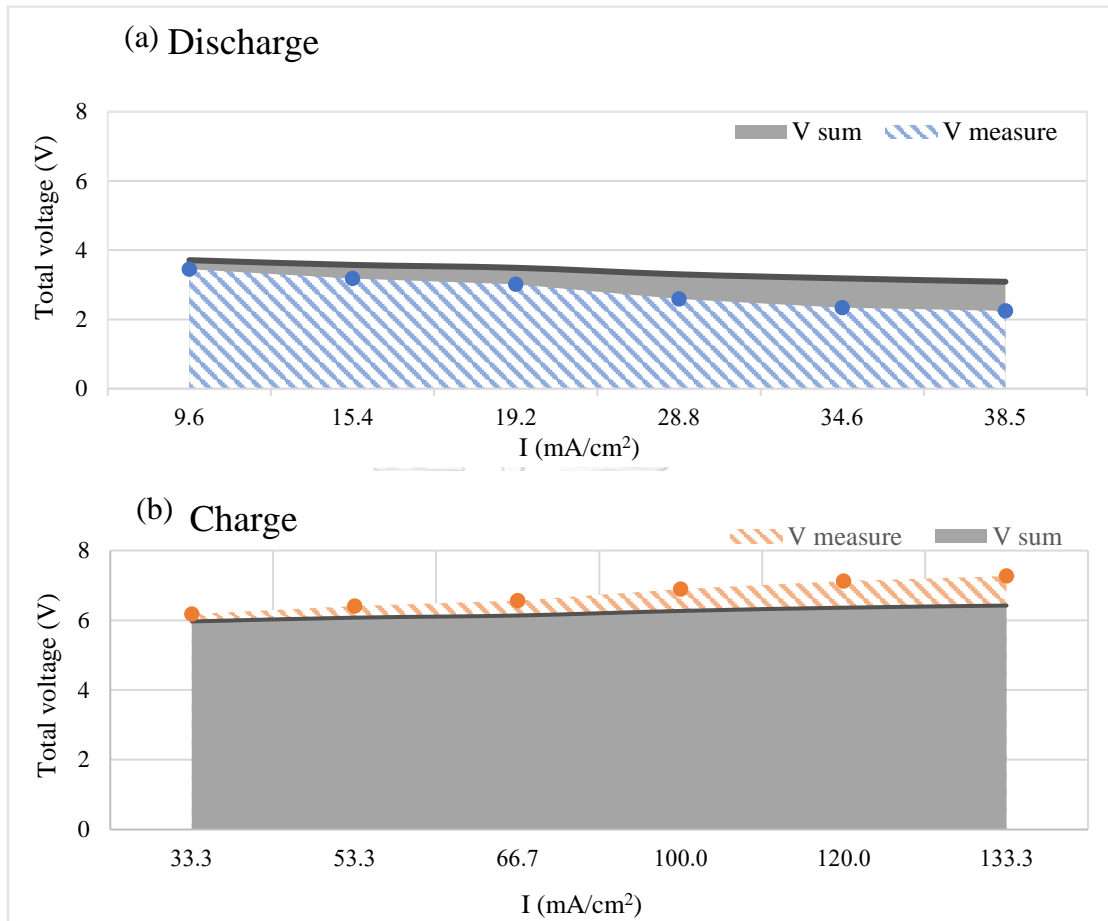
*Figure 4.13 The experimental data comparison of (a) discharge and (b) charge
voltage of 3-cells between measurement voltage of 3-cells (line) and summation
voltage of each cell (gray)*

From experiment, voltage that measures from 3-cells integrated battery not
equal to summation voltage of each cell. In figure 4.13a (voltage during discharge),
total voltage value is lower than summation voltage of each cell. The gap between
total voltage and summation voltage increases due to increasing of current. In figure
4.13b (voltage during charging), total voltage value is higher than summation voltage
of each cell. Because of resistance from Amp meter, wire and contact resistance
generate 0.45 Ω leading to voltage loss in system.

4.2.5 The effect of electrolyte flow rate

Figure 4.14 The simulation data of discharging process which comparing (a) discharging current and (b) coulombic efficiency at 25 mA/cm^2 as a function of electrolyte flow rate

CHULALONGKORN UNIVERSITY

From figure 4.14, battery connecting in series with electrolyte flow system generates leakage current. From figure 4.14a, the connection of 3 cells symmetrically leads to equal value of current in battery I_{z1}, I_{z3} and highest current loss in I_{z2}.

When increase flow rate, current in each cell still be the same but lead to changing of coulombic efficiency. For discharging, coulombic efficiency a bit decrease. Because of flow rate increases, not only reduction of zincate ion accumulation at zinc surface electrode, but also increase corrosion.

While discharging, hydroxide on the zinc electrode surface is used. But, at high flow rate, hydroxide has high rate of diffusion from bulk to surface. The corrosion from HER strongly depends on hydroxide. So, when hydroxide increases, HER increases. The concentration of hydroxide on the zinc electrode surface of the middle cells of stack shown in figure 4.15.

Figure 4.15 The concentration of hydroxide on the surface while discharging at difference electrolyte flow rate

Figure 4.16 The simulation data of charging process which comparing (a) charging current and (b) coulombic efficiency at 25 mA/cm^2 as a function of electrolyte flow rate

For charging, coulombic efficiency increase significantly because of flow rate increase. At high flow rate, zincate has high rate of diffusion from bulk to surface. The sufficient zincate that can reduce parasitic reaction (HER) according to Lao-atiman, Bumroongsil et al. (2019). The concentration of zincate on the zinc electrode surface of the middle cells of stack shown in figure 4.17.
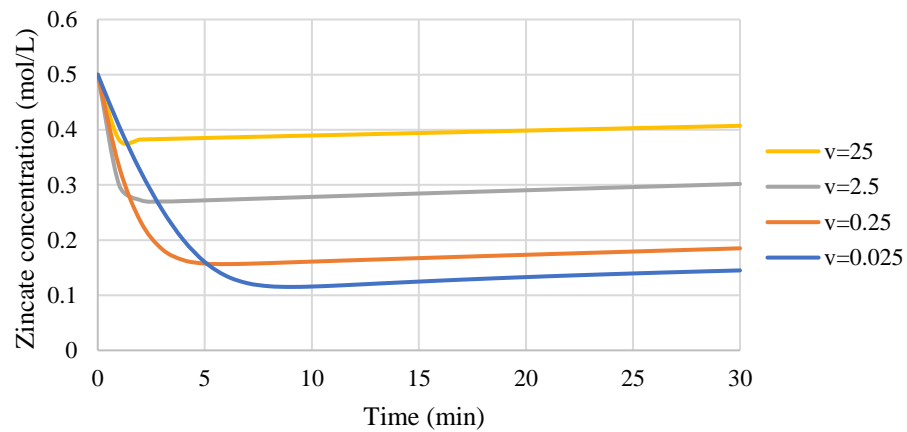
Figure 4.17 The concentration of zincate on the surface while charging at difference electrolyte flow rate
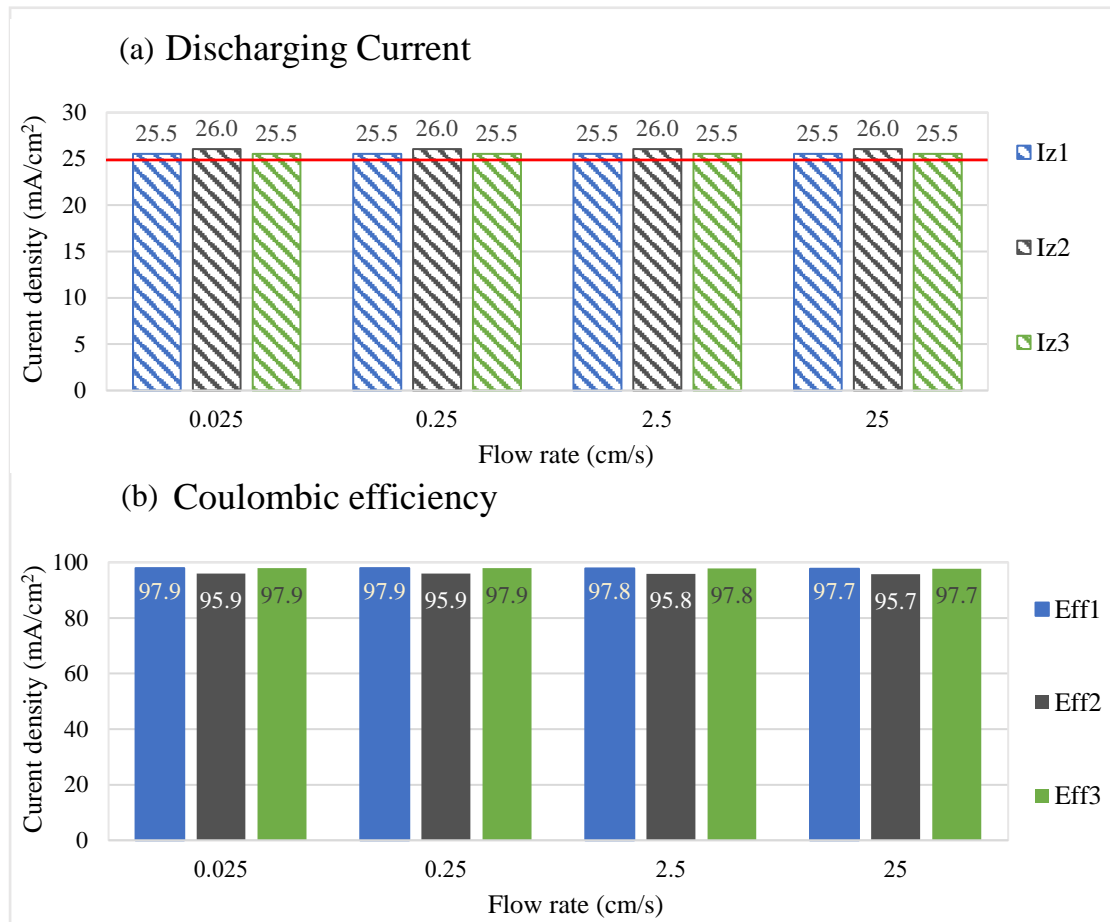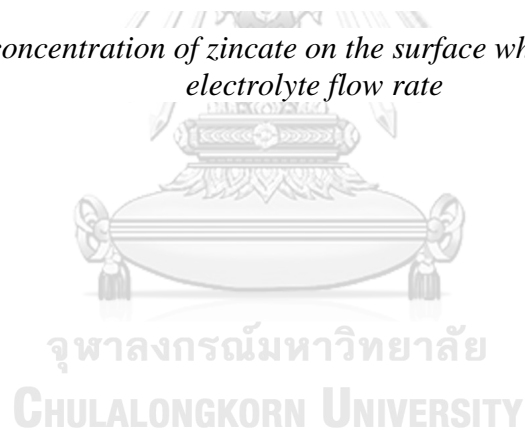
4.2.6 The effect of current density
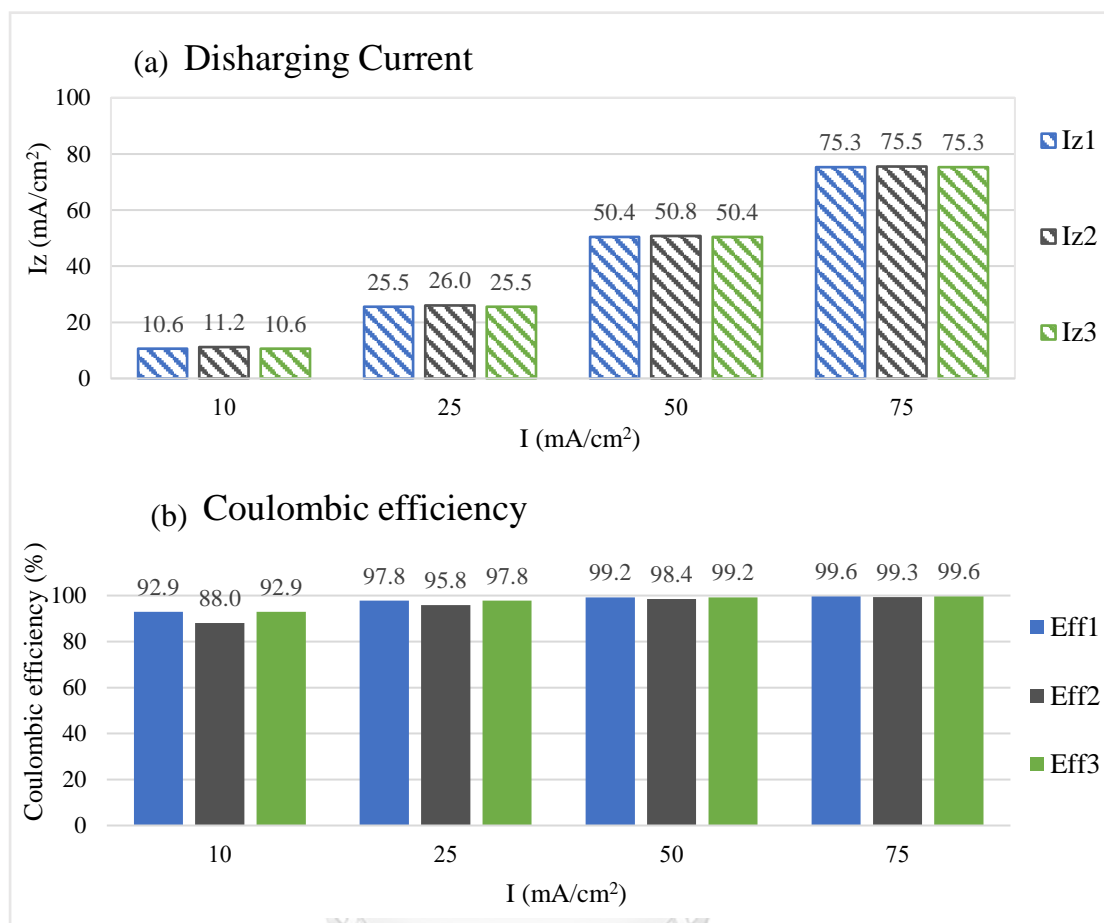
Figure 4.18 The simulation data of discharging process which comparing (a) discharging current and (b) coulombic efficiency at flow rate 2.5 cm/s as a function of applied current density

CHULALONGKORN UNIVERSITY

From figure 4.18a, the current loss of middle cell at 10, 25, 50 and 75 mA/cm^2 are 12%, 4%, 1.6% and 0.7% respectively. In conclude, increasing of discharging current at same flow rate leads to decrease in leakage current. All of battery cells have more nearly same efficiency when increasing current density as shown in figure 4.18b. Due to hydroxide is rapidly used shown in figure 4.19. HER also decreases. This result is simulated at flow rate of 2.5 cm/s for 30 min, there is no zinc oxide occurs at surface of zinc electrode. If using high current in longer time or lower flow rate, it will decrease the efficiency of the system.
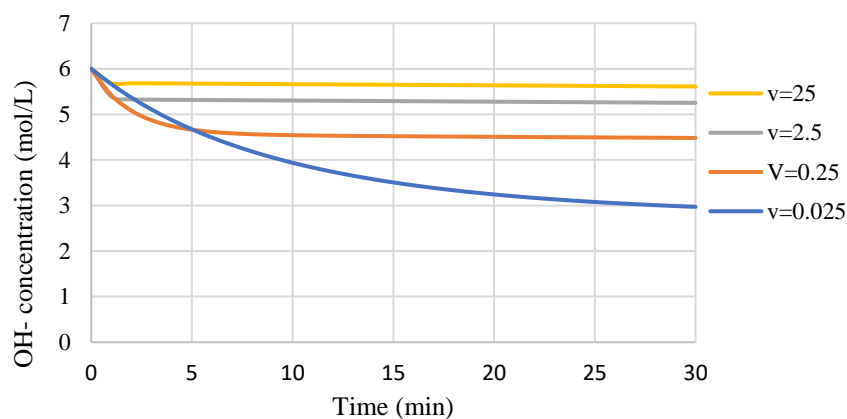
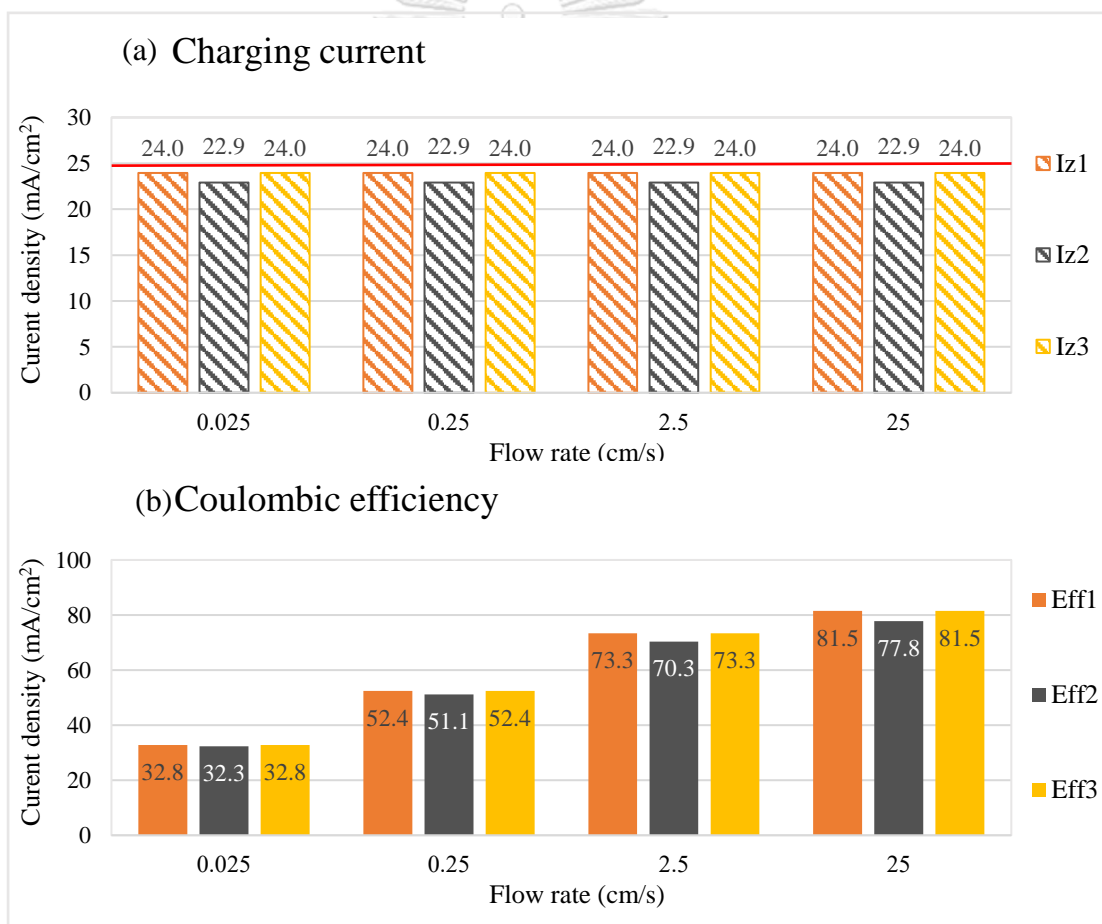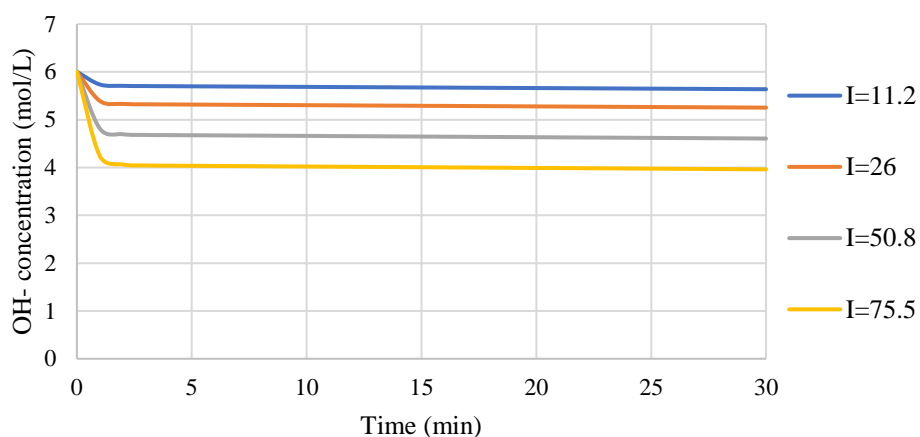*Figure 4.19 The concentration of hydroxide on the surface while discharging at difference current density*

Figure 4.20 The simulation data of charging process which comparing (a) charging current and (b) coulombic efficiency at flow rate 2.5 cm/s as a function of applied current density

From figure 4.20a, the current loss of middle cell at 10, 25, 50 and 75 mA/cm² are 20%, 8.4%, 4.4% and 3.1% respectively. So, increasing of charging current at same flow rate can decrease leakage current. In figure 4.20b, battery efficiency decrease when increase charging current because high current force rapid reaction so zincate at electrode rapidly decreases also. This result agrees with Dundálek, Šnajdr et al. (2017). Lacking of zincate leads to more occurring of HER and reduces inlet electric charge to become zinc metal at surface of electrode as shown in figure 4.21. Besides, at low current density, the leakage current is high. This is the reason why the efficiency drops at 10 mA/cm².
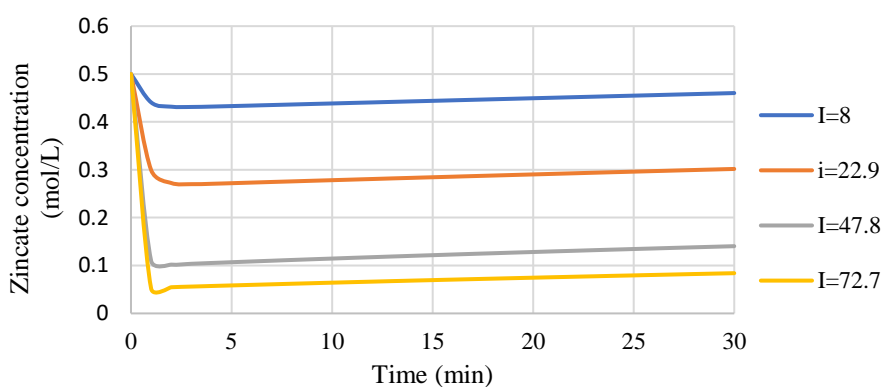
Figure 4.21 The concentration of zincate on the surface while charging at difference current density

4.2.7 The effect of electrolyte flow path resistance
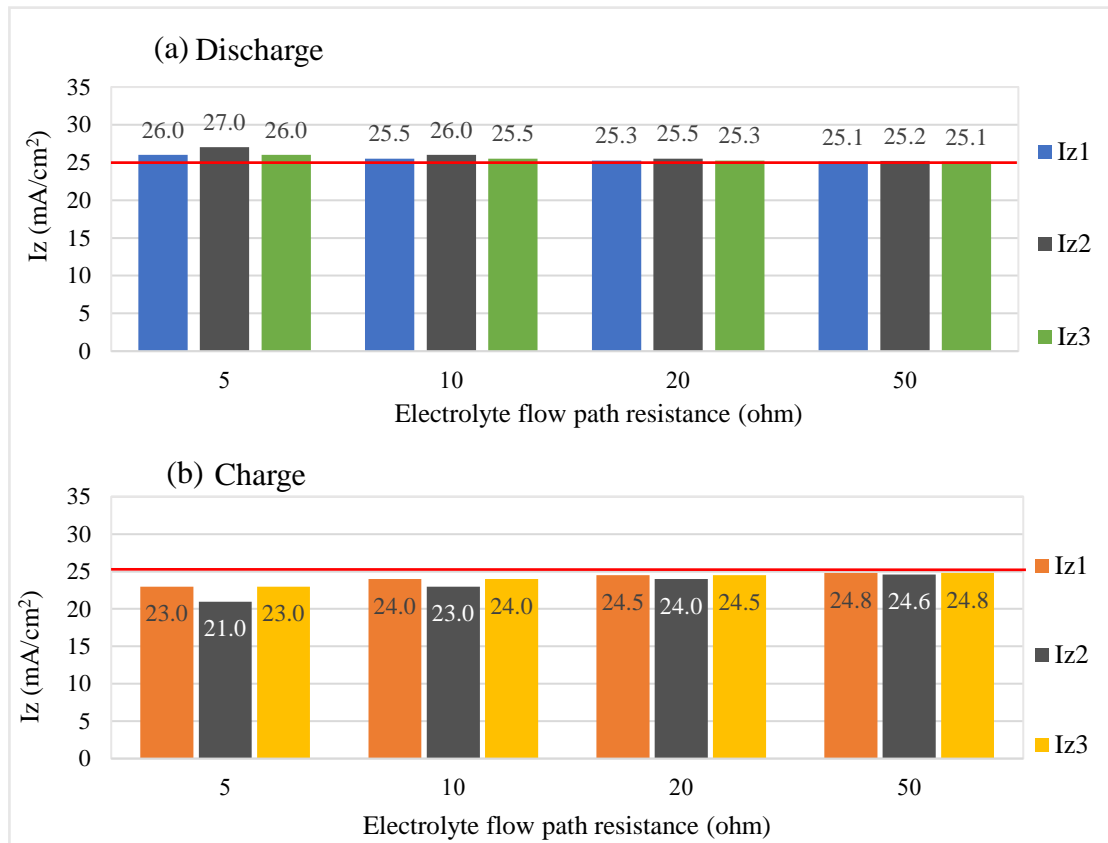
Figure 4.22 The simulation data of (a) discharging and (b) charging process at flow rate 2.5 cm/s and current density 25 mA/cm^2 as a function of electrolyte flow path resistance

Creating stack of battery by connected in series can reduce leakage current by adjusting electrolyte flow path resistance as a result of simulation in figure 4.22. At 5 Ω of discharging process of the middle cell has current loss up to 8%. Charging has current loss up to 16%. Therefore, the operation of stack of battery in series can increase performance by increase electrolyte flow path resistance. The results agree with Prokopius (1976). They recommend designing the long and small electrolyte line in order to reduce shunt current. However, shunt current can be reduced by increasing electrolyte flow path resistance. It must be overcome by increasing pumping power.

And, from König, Suriyah et al. (2015) work, they investigated the diameter of pipe and showed same results. The smaller pipe gives higher efficiency of the battery. On the other hand, Jupudi, Zappi et al. (2007) increased the internal resistance of the cell. It results in increasing shunt current. In addition, they found that the shunt current decreases with increasing resistance non-linearly. If resistance increases beyond the limit, overall loss due to shunt currents reduces to zero.

4.2.8 The effect of number of connected cells
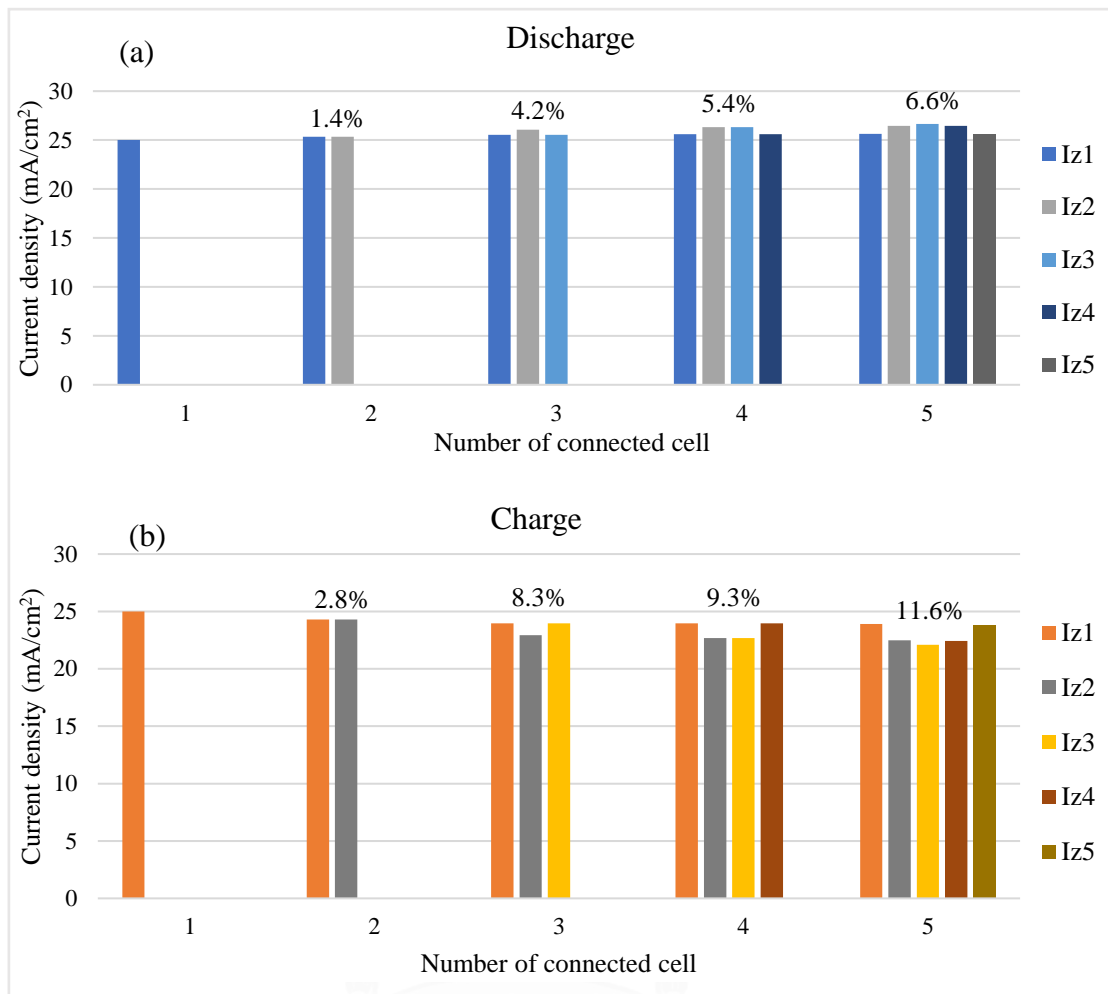
Figure 4.23 The simulation data of (a) discharging and (b) charging process at flow rate 2.5 cm/s and current density 25 mA/cm² varying the number of connected cells in series

Figure 4.23 shows the current in each cell when connected in series for both charging and discharging. When the number of cells increases, it will increase leakage current (König, Suriyah et al. 2015). Loss of current (shown at top of graph) is calculated based on the middle cell which has the highest current loss.

4.3 Connected cells in parallel

The experiment of 3 cells battery in parallel is created follow topic 3.13. This system has equivalent circuit and connected with 3 Amp meters to measure current flow in each cell as shown in figure 4.24.
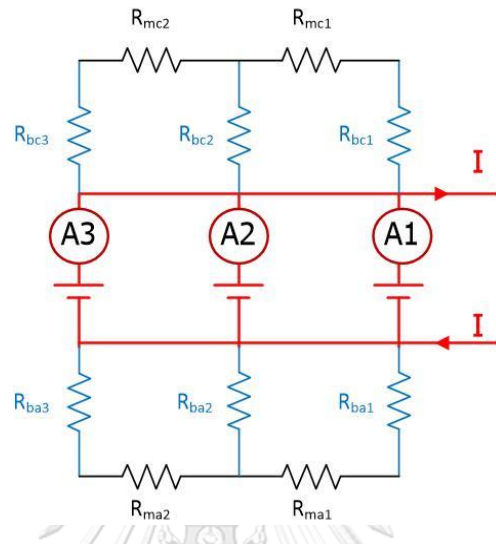
Figure 4.24 The equivalent electric circuit of 3-cells in parallel with current direction, resistance and amp meters

4.3.1 The experiment of 3-cells connected in parallel

Battery connected in parallel with common electrolyte flow system. From figure 4.24, current can flow instantly into battery. The current flow in the battery divide into 3 portions depends on resistance. Current flows to low internal resistance of the battery better than high internal resistance of the battery.
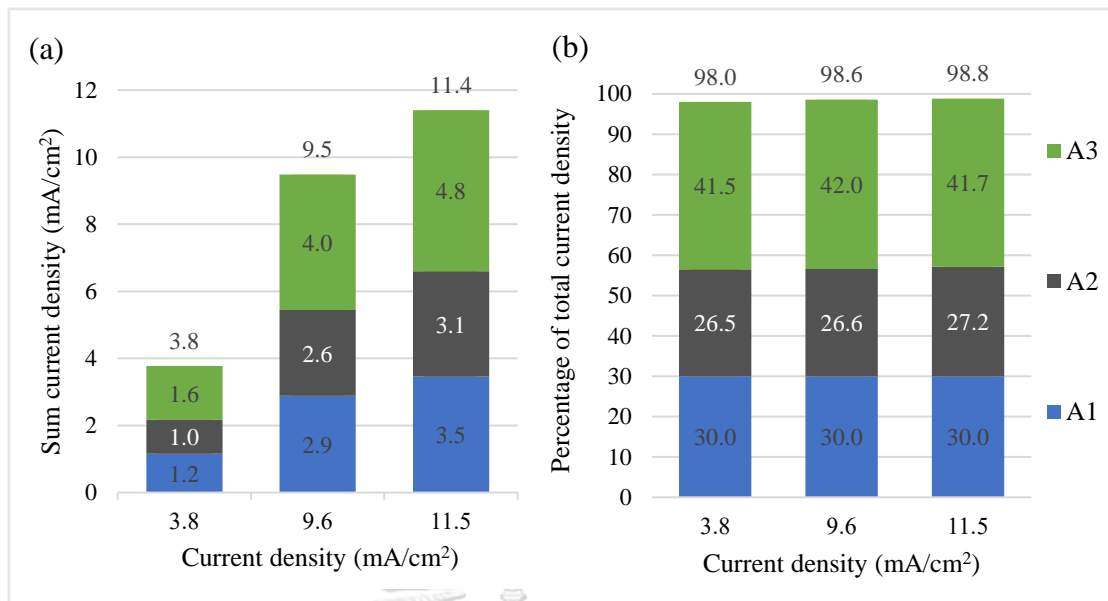
Figure 4.25 The experimental data of discharging current density of each cell which connected in parallel at flow rate 0.25 cm/s showed in (a) current density (b) percentage of total current density

From experiment by connecting cell in parallel in figure 4.24, The current is measured from amp meter shown in figure 4.25a and calculate in percentage in figure 4.25b. Battery 3 can discharge better than battery 1 and 2 which shows that discharging ability relates to battery fabrication.

จุฬาลงกรณ์มหาวิทยาลัย

CHULALONGKORN UNIVERSITY

(a)

(b)
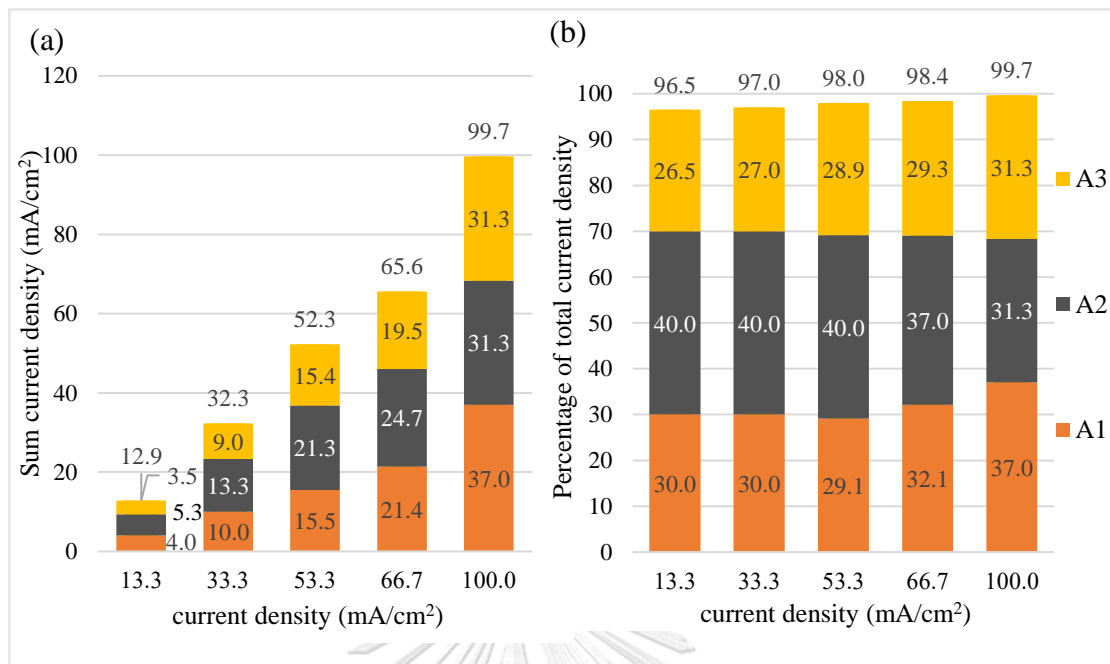
Figure 4.26 The experimental data of charging current density of each cell which connected in parallel at flow rate 0.25 cm/s

During charging, proportions of current flow into each cell has different value but this proportion is constant even increasing input current because resistance of battery of each cell have different value. Summation of inlet current to each cell is nearly same with overall charging current.
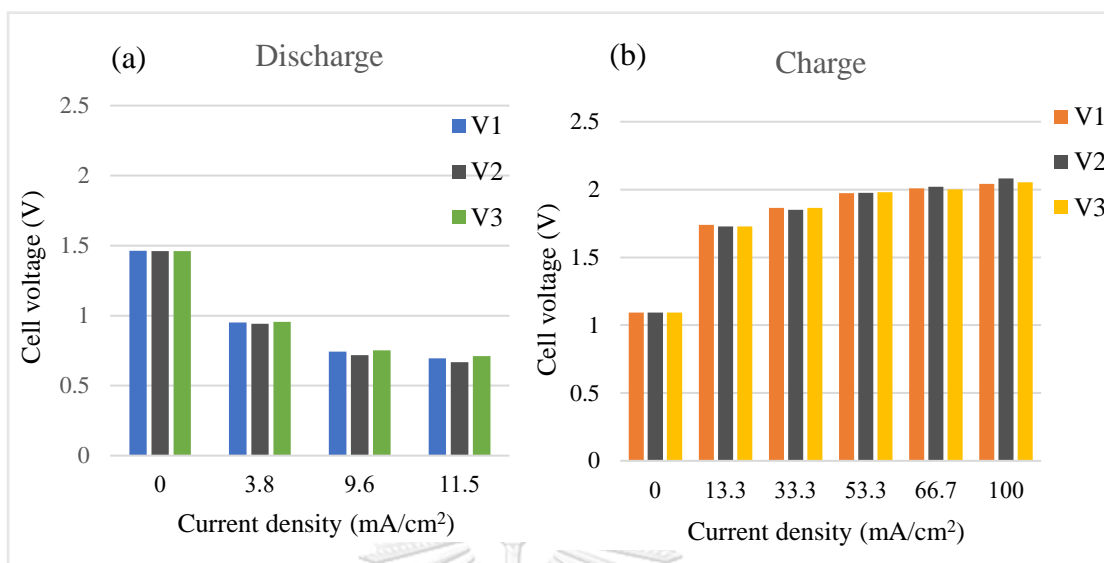
Figure 4.27 The experimental data voltage of each cell with (a) discharging process and (b) charging process which connected in parallel at flow rate 0.25 cm/s as a function of current density

Figure 4.27 shows cell voltage of each cell from experiment, during discharging (figure 4.27a), each battery has same initial voltage and decreases when discharging current increase. Each cell has different reduction of discharging current because each cell has different discharging ability. During charging (figure 4.27b), each cell has same charging current and voltage even charging current increase.

Chapter 5

Conclusion

In this work, zero-dimension models of tri-electrode zinc-air battery with flowing electrolyte was developed. The experiments of cylindrical zinc-air flow battery were conducted to collecting the polarization data. These results were used to fit with the simulation data to validate the model. Some parameters were adjusted until fitting the graphs. The model was validated and it was used to produce the stack of battery.

3-cell of battery connected in series was developed and experiment. The result that measure from amp meter was compared with simulation results and have same value. This model has high accuracy and it was used to determine the effect of battery cells connected in series. From the research, low charging current (9.6 mA/cm^2) have high leakage current up to 13%. When discharge current reaches 38.5 mA/cm^2, leakage current reduces to 2%. Charging also has the same result. Cell voltage from the experiment is same as model at low current density. Differences increase when increasing current density. Due to resistance occur in battery. Overall voltage from measurement doesn't have same value as summation of each cell voltage (ideal series connected). Because in experiment have amp meter and addition wire which increase resistance that leads to voltage loss.

Not only comparing model with experiment data but also use model for investigating the effect of electrolyte flow rate, charge-discharge current density, electrolyte flow path resistance and the number of connected cells. The results show that increasing of flow rate has no effect on leakage current. But affect coulombic efficiency (CE). When increasing flow rate, CE of discharging decreases. For charging, when increasing flow rate, CE significantly increases. For current density, increasing of charging and discharging current affect to reduction of leakage current and affect to CE. When discharging with high current density will have high discharging ability. On the other hand, charging with high current density leads to CE reduction. Charging process has the highest CE value at 25 mA/cm^2. For electrolyte flow path resistance, resistance increase leads to decreasing of shunt current. Last, addition number of cells in series increase shunt current

For cells connected in parallel in equivalent circuit, there is no shunt current occurs. From the experiment, the summation of current in 3 cells compare with discharging current or charging current do not have significant difference even each battery has different input current.

Appendix

A1 Flow rate calibration curve

Table A1.1 The experiment data of flow rate calibration

Speed pump (rpm)	Time/10mL (sec)
10	27.71
25	9.75
40	6.02
60	4.6
75	3.57
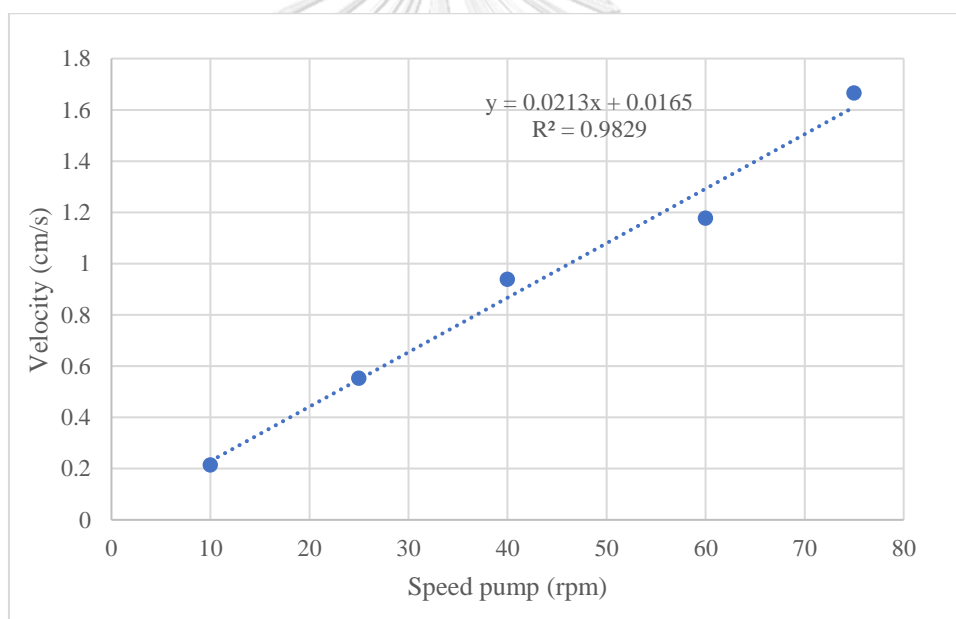
Figure A1.1 Electrolyte flow rate calibration curve of single-cell battery

A2 Polarization data of single-cell battery varying flow rate

Table A2.1 The experiment data of discharging polarization at 10 rpm electrolyte flow

I (mA)	Vcell (V)	Vzn VS Zn (V)	Vair VS Zn (V)	Vzn VS Hg/HgO (V)	Vair VS Hg/HgO (V)
0	1.467	-0.004	1.452	-1.41	0.066
50	1.372	-0.006	1.383	-1.392	-0.013
100	1.338	-0.003	1.332	-1.388	-0.055
200	1.3	0.01	1.304	-1.382	-0.085
400	1.239	0.018	1.254	-1.369	-0.134
600	1.181	0.031	1.216	-1.36	-0.173
800	1.128	0.046	1.17	-1.343	-0.217
1000	1.073	0.053	1.132	-1.324	-0.245
1200	1.028	0.065	1.097	-1.319	-0.282
1400	0.975	0.077	1.056	-1.3	-0.323
1600	0.93	0.092	1.02	-1.294	-0.358
1800	0.885	0.103	0.989	-1.284	-0.39
1900	0.854	0.112	0.948	-1.271	-0.427

Table A2.2 The experiment data of discharging polarization at 35 rpm electrolyte flow

I (mA)	Vcell (V)	Vzn VS Zn (V)	Vair VS Zn (V)	Vzn VS Hg/HgO (V)	Vair VS Hg/HgO (V)
0	1.401	0	1.453	-1.405	-0.01
50	1.372	-0.004	1.392	-1.401	-0.039
100	1.335	-0.001	1.332	-1.395	-0.058
200	1.3	0.02	1.307	-1.386	-0.087
400	1.24	0.023	1.263	-1.366	-0.131
600	1.192	0.04	1.223	-1.359	-0.17
800	1.131	0.042	1.189	-1.345	-0.206
1000	1.08	0.07	1.151	-1.34	-0.24
1200	1.051	0.082	1.114	-1.32	-0.278
1400	0.982	0.084	1.082	-1.29	-0.311
1600	0.929	0.105	1.043	-1.285	-0.339
1800	0.906	0.116	1.021	-1.274	-0.37
1900	0.874	0.126	1.004	-1.269	-0.391

Table A2.3 The experiment data of discharging polarization at 70 rpm electrolyte flow

I (mA)	Vcell (V)	Vzn VS Zn (V)	Vair VS Zn (V)	Vzn VS Hg/HgO (V)	Vair VS Hg/HgO (V)
0	1.491	0	1.49	-1.408	0.082
50	1.4	0.002	1.416	-1.404	-0.004
100	1.342	0.007	1.35	-1.401	-0.05
200	1.306	0.011	1.324	-1.397	-0.088
400	1.239	0.026	1.261	-1.377	-0.138
600	1.19	0.042	1.234	-1.365	-0.171
800	1.132	0.048	1.195	-1.34	-0.208
1000	1.062	0.066	1.16	-1.319	-0.239
1200	1.01	0.075	1.125	-1.309	-0.269
1400	0.985	0.091	1.091	-1.292	-0.303
1600	0.94	0.116	1.06	-1.278	-0.34
1800	0.889	0.118	1.026	-1.27	-0.375
1900	0.878	0.121	1.02	-1.262	-0.383

Table A2.4 The experiment data of charging polarization at 10 rpm electrolyte flow

I (mA)	Vcell (V)	Vzn VS Zn (V)	Vair VS Zn (V)	Vzn VS Hg/HgO (V)	Vair VS Hg/HgO (V)
0	1.816	-0.01	1.789	-1.402	-0.006
50	1.936	-0.034	1.902	-1.408	0.497
100	1.968	-0.052	1.918	-1.422	0.526
200	2.006	-0.079	1.935	-1.452	0.556
400	2.08	-0.125	1.955	-1.497	0.582
600	2.123	-0.16	1.97	-1.537	0.597
800	2.187	-0.194	1.991	-1.571	0.628
1000	2.255	-0.242	2.01	-1.602	0.635
1200	2.305	-0.272	2.02	-1.635	0.645
1400	2.353	-0.311	2.031	-1.667	0.668
1600	2.4	-0.325	2.048	-1.685	0.683
1800	2.452	-0.374	2.058	-1.691	0.722
2000	2.49	-0.392	2.068	-1.715	0.767

Table A2.5 The experiment data of charging polarization at 35 rpm electrolyte flow

I (mA)	Vcell (V)	Vzn VS Zn (V)	Vair VS Zn (V)	Vzn VS Hg/HgO (V)	Vair VS Hg/HgO (V)
0	1.722	-0.013	1.805	-1.402	-0.006
50	1.907	-0.015	1.902	-1.408	0.506
100	1.95	-0.039	1.931	-1.422	0.523
200	2.001	-0.057	1.946	-1.452	0.541
400	2.066	-0.11	1.971	-1.497	0.56
600	2.128	-0.148	1.985	-1.537	0.578
800	2.189	-0.193	2.013	-1.571	0.593
1000	2.237	-0.221	2.039	-1.602	0.6
1200	2.286	-0.258	2.051	-1.635	0.608
1400	2.334	-0.294	2.052	-1.667	0.64
1600	2.384	-0.319	2.072	-1.727	0.67
1800	2.44	-0.328	2.082	-1.736	0.682
2000	2.464	-0.387	2.097	-1.76	0.692

Table A2.6 The experiment data of charging polarization at 70 rpm electrolyte flow

I (mA)	Vcell (V)	Vzn VS Zn (V)	Vair VS Zn (V)	Vzn VS Hg/HgO (V)	Vair VS Hg/HgO (V)
0	1.792	-0.003	1.79	-1.422	0.386
50	1.946	-0.023	1.91	-1.432	0.435
100	1.969	-0.034	1.929	-1.436	0.489
200	2.017	-0.078	1.951	-1.47	0.526
400	2.085	-0.092	1.954	-1.5	0.554
600	2.148	-0.126	1.964	-1.514	0.57
800	2.207	-0.163	1.981	-1.52	0.599
1000	2.27	-0.229	2	-1.573	0.589
1200	2.327	-0.245	2.011	-1.601	0.605
1400	2.371	-0.293	2.01	-1.699	0.622
1600	2.425	-0.343	2.03	-1.765	0.632
1800	2.464	-0.367	2.06	-1.8	0.65
2000	2.514	-0.462	2.1	-1.839	0.721

A3 Experimental data of 3-cell battery connected in series

Table A3.1 The experiment data of discharging polarization at 35 rpm total electrolyte flow

I (mA)	Vz1 (V)	Vz2 (V)	Vz3 (V)	A1 (mA)	A2 (mA)	V total (V)
0	1.393	1.378	1.389	0	0	4.18
200	1.246	1.219	1.246	228	210	3.75
500	1.201	1.17	1.203	527	520	3.45
800	1.175	1.14	1.176	823	820	3.184
1000	1.114	1.072	1.117	1020	1010	3.011
1500	1.079	1.025	1.081	1514	1510	2.59
1800	1.052	0.974	1.061	1800	1812	2.336
2000	1.393	1.378	1.389	2009	2000	2.25

Table A3.2 The experiment data of discharging polarization at 70 rpm total electrolyte flow

I (mA)	Vz1 (V)	Vz2 (V)	Vz3 (V)	A1 (mA)	A2 (mA)	V total (V)
0	1.44	1.38	1.4	0	0	4.19
200	1.24	1.22	1.24	229	230	3.75
500	1.2	1.17	1.2	526	520	3.39
800	1.17	1.14	1.17	822	820	3.05
1000	1.11	1.07	1.11	1017	1010	2.9
1500	1.08	1.03	1.08	1512	1510	2.56
1800	1.04	0.98	1.05	1805	1800	2.17
2000	1.44	1.38	1.4	2003	2000	1.81

Table A3.3 The experiment data of charging polarization at 35 rpm total electrolyte flow

I (mA)	Vz1 (V)	Vz2 (V)	Vz3 (V)	A1 (mA)	A2 (mA)	V total (V)
0	2.069	2.026	2.029	0	0	6.1
200	1.942	1.929	1.922	155	150	5.85
500	2.012	1.982	1.973	451	440	6.18
800	2.05	2.016	2.01	751	740	6.41
1000	2.071	2.037	2.03	950	940	6.57
1500	2.118	2.077	2.074	1452	1440	6.9
1800	2.151	2.104	2.107	1752	1740	7.13
2000	2.172	2.122	2.129	1949	1940	7.27

Table A3.4 The experiment data of charging polarization at 70 rpm total electrolyte flow

I (mA)	Vz1 (V)	Vz2 (V)	Vz3 (V)	A1 (mA)	A2 (mA)	V total (V)
0	1.82	1.810	1.815	0	0	5.32
200	1.93	1.93	1.91	151	140	5.85
500	1.99	1.97	1.97	448	440	6.14
800	2.03	2.01	2	748	740	6.4
1000	2.06	2.03	2.02	946	940	6.56
1500	2.12	2.07	2.07	1447	1430	6.93
1800	2.15	2.1	2.1	1745	1740	7.15
2000	2.17	2.12	2.12	1944	1920	7.29

A4 Experimental data of 3-cell battery connected in parallel

Table A4.1 The experiment data of discharging polarization at 35 rpm total electrolyte flow

I (mA)	Vz1 (V)	Vz2 (V)	Vz3 (V)	A1 (mA)	A2 (mA)	A3 (mA)
0	1.463	1.462	1.462	0	0	0
200	0.951	0.941	0.955	60	53	83
500	0.743	0.717	0.753	150	133	210
600	0.694	0.667	0.712	180	163	250

Table A4.2 The experiment data of charging polarization at 35 rpm total electrolyte flow

I (mA)	Vz1 (V)	Vz2 (V)	Vz3 (V)	A1 (mA)	A2 (mA)	A3 (mA)
0	1.094	1.093	1.092	0	0	0
200	1.739	1.727	1.727	60	80	53
500	1.865	1.851	1.865	150	200	135
800	1.973	1.975	1.981	233	320	231
1000	2.009	2.02	2.002	321	370	293
1500	2.041	2.081	2.054	555	470	470
1800	2.05	2.126	2.08	659	530	598
2000	2.058	2.149	2.094	710	580	699

REFERENCES

Amunátegui, B., A. Ibáñez, M. Sierra and M. Pérez (2018). "Electrochemical energy storage for renewable energy integration: zinc-air flow batteries." Journal of Applied Electrochemistry **48**(6): 627-637.

Bidault, F., D. J. L. Brett, P. H. Middleton and N. P. Brandon (2009). "Review of gas diffusion cathodes for alkaline fuel cells." Journal of Power Sources **187**(1): 39-48.

Bockelmann, M., L. Reining, U. Kunz and T. Turek (2017). "Electrochemical characterization and mathematical modeling of zinc passivation in alkaline solutions: A review." Electrochimica Acta **237**: 276-298.

Clark, S., A. Latz and B. Horstmann (2018). "A Review of Model-Based Design Tools for Metal-Air Batteries." Batteries **4**(1).

Deiss, E., F. Holzer and O. Haas (2002). "Modeling of an electrically rechargeable alkaline Zn–air battery." Electrochimica Acta **47**(25): 3995-4010.

Dundálek, J., I. Šnajdr, O. Libánský, J. Vrána, J. Pocedič, P. Mazúr and J. Kosek (2017). "Zinc electrodeposition from flowing alkaline zincate solutions: Role of hydrogen evolution reaction." Journal of Power Sources **372**: 221-226.

Gavrilovic-Wohlmuther, A., A. Laskos, C. Zelger, B. Gollas and A. H. Whitehead (2015). "Effects of Electrolyte Concentration, Temperature, Flow Velocity and Current Density on Zn Deposit Morphology." Energy and Power Engineering **9**: 1019-1028.

Gilliam, R. J., J. W. Graydon, D. W. Kirk and S. J. Thorpe (2007). "A review of specific conductivities of potassium hydroxide solutions for various concentrations and temperatures." International Journal of Hydrogen Energy **32**(3): 359-364.

Hong, W. (2016). A Horizontal Three-Electrode Structure for Zinc-Air Batteries with Long-Term Cycle Life and High Performance.

Jung, C.-Y., T.-H. Kim, W.-J. Kim and S.-C. Yi (2016). "Computational analysis of the zinc utilization in the primary zinc-air batteries." Energy **102**: 694-704.

Jupudi, R., G. Zappi and R. Bourgeois (2007). "Prediction of shunt currents in a bipolar electrolyzer stack by difference calculus." Journal of Applied Electrochemistry **37**: 921-931.

Khor, A., P. Leung, M. R. Mohamed, C. Flox, Q. Xu, L. An, R. G. A. Wills, J. R. Morante and A. A. Shah (2018). "Review of zinc-based hybrid flow batteries: From fundamentals to applications." Materials Today Energy **8**: 80-108.

Lao-atiman, W., K. Bumroongsil, A. Arpornwichanop, P. Bumroongsakulsawat, S. Olaru and S. Kheawhom (2019). "Model-Based Analysis of an Integrated Zinc-Air Flow Battery/Zinc Electrolyzer System." **7**(15).

Li, Y. and H. Dai (2014). Recent advances in Zinc-air batteries.

Mao, Z. (1992). "Mathematical Modeling of a Primary Zinc/Air Battery." Journal of The Electrochemical Society **139**(4).

Mu¨Ller, S., O. Haas, C. Schlatter and C. Comninellis (1998). "Development of a 100 W rechargeable bipolar zinc/oxygen battery." Journal of Applied Electrochemistry **28**(3): 305-310.

Pichler, B., B. S. Berner, N. Rauch, C. Zelger, H.-J. Pauling, B. Gollas and V. Hacker (2018). "The impact of operating conditions on component and electrode development for zinc-air flow batteries." Journal of Applied Electrochemistry **48**(9): 1043-1056.

Riede, J.-C., T. Turek and U. Kunz (2018). "Critical zinc ion concentration on the electrode surface determines dendritic zinc growth during charging a zinc air battery."

Electrochimica Acta **269**: 217-224.

Schröder, D. (2016). Analysis of Reaction and Transport Processes in Zinc Air Batteries.

Schröder, D. and U. Krewer (2014). "Model based quantification of air-composition impact on secondary zinc air batteries." Electrochimica Acta **117**: 541-553.

See, D. M. and R. E. White (1997). "Temperature and Concentration Dependence of the Specific Conductivity of Concentrated Solutions of Potassium Hydroxide." Journal of Chemical & Engineering Data **42**(6): 1266-1268.

Stamm, J., A. Varzi, A. Latz and B. Horstmann (2017). "Modeling nucleation and growth of zinc oxide during discharge of primary zinc-air batteries." Journal of Power Sources **360**: 136-149.

Sunu, W. G. and D. N. Bennion (1980). "TRANSIENT AND FAILURE ANALYSES OF THE POROUS ZINC ELECTRODE - 1. THEORETICAL." Journal of the Electrochemical Society **127**: 2007-2016.

Tromans, D. (1998). "Oxygen solubility modeling in inorganic solutions: concentration, temperature and pressure effects." Hydrometallurgy **50**(3): 279-296.

Vatsalarani, J., D. d. Trivedi, K. Ragavendran and P. C. Warrier (2005). Effect of Polyaniline Coating on "Shape Change" Phenomenon of Porous Zinc Electrode.

Wandschneider, F. T., S. Röhm, P. Fischer, K. Pinkwart, J. Tübke and H. Nirschl (2014). "A multi-stack simulation of shunt currents in vanadium redox flow batteries." Journal of Power Sources **261**: 64-74.

Wang, K., P. Pei, Z. Ma, H. Chen, H. Xu, D. Chen and X. Wang (2015). "Dendrite growth in the recharging process of zinc–air batteries." Journal of Materials Chemistry A **3**(45): 22648-22655.

Wang, K., P. Pei, Z. Ma, H. Xu, P. Li and X. Wang (2014). "Morphology control of zinc regeneration for zinc–air fuel cell and battery." Journal of Power Sources **271**: 65-75.

Zhu, A. L., D. Duch, G. A. Roberts, S. X. X. Li, H. Wang, K. Duch, E. Bae, K. S. Jung, D. Wilkinson and S. A. Kulinich (2015). "Increasing the Electrolyte Capacity of Alkaline Zn–Air Fuel Cells by Scavenging Zincate with Ca(OH)2." ChemElectroChem **2**(1): 134-142.

Zhu, X. M., H. X. Yang, X. P. Ai, J. X. Yu and Y. L. Cao (2003). "Structural and electrochemical characterization of mechanochemically synthesized calcium zincate as rechargeable anodic materials." Journal of Applied Electrochemistry **33**(7): 607-612.

VITA

NAME	Kanya Bumroongsil
DATE OF BIRTH	19 September 1993
PLACE OF BIRTH	Bangkok Thailand
INSTITUTIONS ATTENDED	Chulalongkorn university
HOME ADDRESS	60 Ramintra 14/17 Tharaeng Bangkhen Bangkok 10230